Basolateral sorting of chloride channel 2 is mediated by interactions between a dileucine motif and the clathrin adaptor AP-1

Erwin de la Fuente-Ortega[a,*,†], Diego Gravotta[a,*], Andres Perez Bay[a], Ignacio Benedicto[a], Jose Maria Carvajal-Gonzalez[a,‡], Guillermo L. Lehmann[a], Carlos F. Lagos[b,c], and Enrique Rodríguez-Boulan[a]

[a]Dyson Vision Research Institute, Department of Ophthalmology, Weill Cornell Medical College, New York, NY 10065; [b]Department of Endocrinology, School of Medicine, Pontificia Universidad Católica de Chile, Santiago Centro 8330074, Santiago, Chile; [c]Facultad de Ciencia, Universidad San Sebastián, Providencia 7510157, Santiago, Chile

ABSTRACT **In spite of the many key cellular functions of chloride channels, the mechanisms that mediate their subcellular localization are largely unknown. ClC-2 is a ubiquitous chloride channel usually localized to the basolateral domain of epithelia that regulates cell volume, ion transport, and acid–base balance; mice knocked out for ClC-2 are blind and sterile. Previous work suggested that CLC-2 is sorted basolaterally by TIFS^{812}LL, a dileucine motif in CLC-2's C-terminal domain. However, our in silico modeling of ClC-2 suggested that this motif was buried within the channel's dimerization interface and identified two cytoplasmically exposed dileucine motifs, ESMI^{623}LL and QVVA^{635}LL, as candidate sorting signals. Alanine mutagenesis and trafficking assays support a scenario in which ESMI^{623}LL acts as the authentic basolateral signal of ClC-2. Silencing experiments and yeast three-hybrid assays demonstrated that both ubiquitous (AP-1A) and epithelium-specific (AP-1B) forms of the tetrameric clathrin adaptor AP-1 are capable of carrying out basolateral sorting of ClC-2 through interactions of ESMI^{623}LL with a highly conserved pocket in their γ1-σ1A hemicomplex.**

Monitoring Editor
Keith E. Mostov
University of California, San Francisco

Received: Jan 27, 2015
Revised: Feb 25, 2015
Accepted: Feb 25, 2015

INTRODUCTION

Chloride channels control a wide array of key cellular functions, such as muscle and nerve excitability, transepithelial salt and water transport, cell volume, and acidification of intracellular organelles. Not surprisingly, their mutations lead to a wide spectrum of human diseases (Jentsch *et al.*, 2005; Stölting *et al.*, 2014). ClC-2 is a ubiquitous voltage-gated chloride channel particularly abundant in epithelial tissues (Gründer *et al.*, 1992; Thiemann *et al.*, 1992) and is believed to play key roles in transepithelial chloride transport processes in response to hyperpolarization, cell swelling, and extracellular acidification (Jentsch, 2005). ClC-2 belongs to a family of nine mammalian chloride channels: whereas ClC-2, 1, Ka, and Kb preferentially localize to the plasma membrane, the other family members, ClC-3–7, localize to endosomal compartments (Jentsch, 2008). ClC-2 knockout in mice causes blindness and male sterility (Bosl *et al.*, 2001; Nehrke *et al.*, 2002; Edwards *et al.*, 2010), consistent with its expression in epithelial cells that form blood–tissue barriers in retina and testis, that is, retinal pigment epithelium (RPE) and Sertoli cells (Jentsch, 2005; Strauss, 2005). Chloride channels are usually dimers, with each monomer having its own pore (Jentsch, 2002). Based on the crystal structure of structurally similar bacterial channels, ClC-2 is believed to be a polytopic protein, with 18 α-helical segments (A–R) and a large, cytoplasmically exposed C-terminal segment containing two cystathionine β-synthase (CBS) domains, CBS1 and CBS2 (Peña-Münzenmayer *et al.*, 2005; Figure 1A). Mutational studies and structural modeling suggest that the CBS domains

This article was published online ahead of print in MBoC in Press (http://www.molbiolcell.org/cgi/doi/10.1091/mbc.E15-01-0047) on March 4, 2015.

*These authors contributed equally.

Present addresses: †Departamento de Ciencias Biomédicas, Facultad de Medicina, Universidad Católica del Norte, Coquimbo 1781421, Chile; ‡Departamento de Bioquimica y Biologia Molecular y Genetica, Unidad de Bioquimica y Biologia Molecular, Facultad de Ciencias, Universidad de Extremadura, 06080-Badajoz, Spain.

Address correspondence to: Enrique Rodríguez-Boulan (boulan@med.cornell.edu), Diego Gravotta (dig2003@med.cornell.edu), Erwin de la Fuente-Ortega (edelafuente@ucn.cl).

Abbreviations used: AP-1A, AP-1B, heterotetrameric clathrin adaptor protein complex 1A and 1B, respectively; CBS, cystathionine beta synthase; LLC-PK1, Lilly Laboratory porcine kidney 1; MDCK, Madin–Darby canine kidney; Nef, negative regulatory factor; p75NTR, p75 neurotrophin receptor; SBAS, surface biotinylation avidin shift

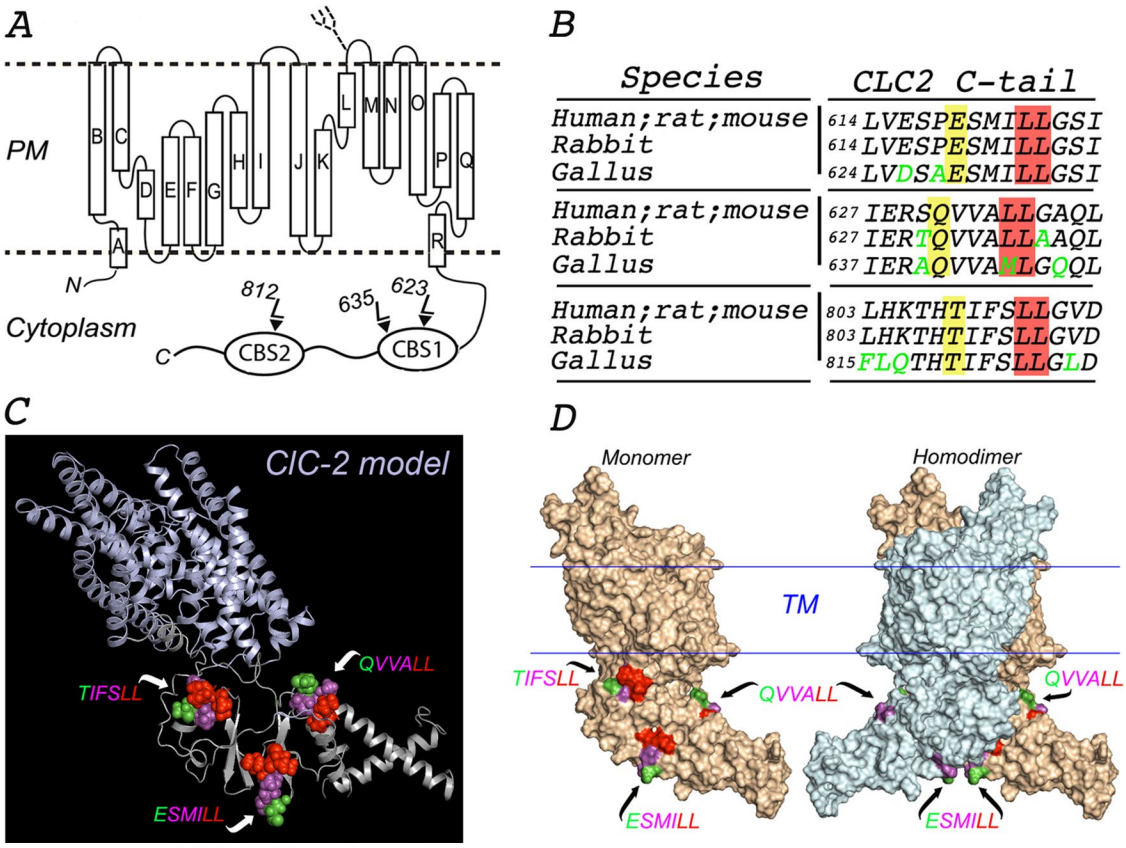

FIGURE 1: In silico molecular model of ClC-2. (A) Proposed topology of human ClC-2. ClC-2 displays 18 α-helices (A–R) that span the membrane, both N- and C-terminus ends facing the cytoplasm. The C-terminus of ClC-2 contains the CBS1 and CBS2 domains, which display two and one dileucine motifs, respectively. A single N-linked glycan is present on the short luminal loop between the L and M α-helices, as indicated. (B) Multiple sequence alignment using Clustal Omega program (UniProt) with sequences from the indicated species (P51788, human; P35525, rat; Q9R0A1, mouse; P51789, rabbit; XP 423073.4, gallus). The amino acid sequences around each of the three dileucine motifs in the cytoplasmic tail of ClC-2 are conserved in mammals (human, rat, mouse, and rabbit). One of the two leucines in the QVVA^{645}LL motif is changed to a methionine (QVVA^{645}ML) in birds (gallus). Conserved residues are shown in black, and nonconserved residues are shown in green. The critical leucine pair and residues at position −4 are shaded in red and yellow, respectively. (C) Combined cartoon-rendered structure in a monomer of ClC-2 displaying the three dileucine motifs in a sphere format. We modeled the structure of ClC-2 (UniProt P51788) using MODELLER and available crystal structure information for the transmembrane and extracellular domains of CmClC (3ORG), EcClC (1OTS), and StCLC (1KPL) and for the CBS domains of ClC-Ka (2PFI) and ClC-0 (2D4Z). (D) Surface-rendered structure of ClC-2 monomer (left) and homodimer (right) displaying the three dileucine motifs. TIFS ^{812}LL is present in a region of CBS2 that participates in the dimerization of the channel and is thus hidden in the dimer. For each motif, essential L residues are represented in red, nonessential variable residues at −1, −2, and −3 positions are displayed in magenta, and the residues at the −4 position are shown in green.

modulate the trafficking and channel activity of ClC-2 (Peña-Münzenmayer *et al.*, 2005; Garcia-Olivares *et al.*, 2008; Feng *et al.*, 2010).

The polarized localization of ClC-2 in epithelial cells was initially controversial, with some studies reporting an apical localization in lung alveolar cells (Murray *et al.*, 1995; Blaisdell *et al.*, 2000) and intestinal cells (Gyömörey *et al.*, 2000), which made it a good candidate to complement cystic fibrosis transmembrane conductance regulator' secretory function, whereas other studies reported a basolateral localization in intestinal cells compatible with absorption processes (Catalán *et al.*, 2002, 2004; Lipecka *et al.*, 2002). However, an immunocytochemical and transfection study (Peña-Münzenmayer *et al.*, 2005) unequivocally established that ClC-2 localizes to the basolateral plasma membrane of absorptive epithelial cells of rat and mouse colon and small intestine. Furthermore, their mutagenesis experiments identified a dileucine motif, TIFS^{812}LL, implicated in the basolateral localization of ClC-2 in Madin–Darby canine kidney (MDCK) cells and suggested a role of the clathrin adaptor AP-1B in the basolateral sorting of the channel.

Dileucine-based sorting signals fall into two main classes, defined by the consensus motifs DXXLL and [D/E]XXXL[L/I] (D, aspartate; E, glutamate; L, leucine; I, isoleucine). DXXLL motifs occur within the cytosolic tails of intracellular sorting receptors such as mannose-6-phosphate receptors (Johnson and Kornfeld, 1992) and are known to bind to the Vps27, Hrs, and Stam domain of Golgi-localized, γ-ear-containing, ARF-binding proteins (Puertollano *et al.*, 2001; Zhu *et al.*, 2001). [D/E]XXXL[L/I] motifs (Letourneur and Klausner, 1992) are present in the cytoplasmic domains of many transmembrane proteins targeted to endosomes, lysosomes, and lysosome-related organelles (Bonifacino and Traub, 2003). Both types of dileucine motifs are known to participate in clathrin-mediated post-Golgi sorting of membrane proteins to endosomes and

Protein	BL signal and key residues	Endocytic activity	BL sorting machinery	Reference
ClC-2	TIFS**LL**	?	AP-1B	Peña-Münzenmayer *et al.* (2005)
ClC-2	ESMI**LL**	?	AP-1A, AP-1B	This study
IgG Fc receptor B-cell 1 (FcRII-B1)	ITYS**LL**	Yes	?	Hunziker and Fumey (1994)
Neonatal IgG-Fc receptor (FcRn)	**D**SGD**LL**	Yes	?	Newton *et al.* (2005)
Glycine transporter 1b (GLYT 1b)	DGDT**LL**	?	?	Poyatos *et al.* (2000)
Lutheran antigen(Lu)	EQTG**LL**	?	?	Nemer *et al.* (1999)
Melanoma cell adhesion molecule isoform 1 (MCam-1)	EEAG**LL**	?	?	Guezguez *et al.* (2006)
Cu^{2+}-translocating ATPase (ATP7A)	DKHS**LL**	?	?	Greenough *et al.* (2004)
MHC class II invariant chain (MHC-Ii)	DQRD**L**L EQLPM**L**	? ?	?	Simonsen *et al.* (1997)
E-cadherin	VKEP**LL**	?	PIPK-1γ AP-1B	Miranda *et al.* (2001) Ling *et al.* (2007)
IgG Fc receptor B-cell 1 (FcRII-B1)	ITYS**LL**	Yes	?	Hunziker and Fumey (1994)
Glycoprotein 130 (GP130)	STQT**LL**	Yes	?	Doumanov *et al.* (2006)
Ectonucleotide pyrophosphatase/ phosphodiesterase 1 (NPP1)	AAAS**LL**	Yes	?	Bello *et al.* (2001)
Rat sulfate anion transporter 1 (SAT-1)	TAEE**LL**	Yes	?	Regeer and Markovich (2004)

IgG, immunoglobulin G. National Center for Biotechnology Information sequences of [D/E]XXXL[L/I] dileucine motifs in the cytoplasmic domain of indicated transmembrane cargo proteins. Critical residues for basolateral sorting are highlighted in bold.

TABLE 1: Proteins with dileucine-based basolateral sorting signals.

lysosomes (Bonifacino and Traub, 2003; Traub, 2009). Furthermore, [D/E]XXXL[L/I] motifs have been implicated in clathrin-mediated endocytosis (Letourneur and Klausner, 1992) and, relevant to this study, in the post-Golgi sorting of about a dozen basolateral proteins (Table 1). In [D/E]XXXL[L/I] motifs, the leucine–leucine and leucine–isoleucine pairs are critical elements of the signals, whereas the aspartate or glutamate residue at the –4 position is often important but not essential for function (for examples of both cases, see Table 1). Yeast three-hybrid and glutathione *S*-transferase–protein pull-down assays have shown that [D/E]XXXL[L/I] motifs interact with the γ–σ1 hemicomplex of the heterotetrameric clathrin adaptor AP-1 (Janvier *et al.*, 2003; Doray *et al.*, 2007) through conserved residues also present in the equivalent α–σ2 and δ–σ3 hemicomplexes of the clathrin adaptors AP-2 and AP-3 (Kelly *et al.*, 2008; Mattera *et al.*, 2011). Furthermore, it is now clear that AP-1 occurs as a diversity of heterotetramers through combinatorial assembly of various γ and σ1 subunits, encoded by different genes. Relevant to this study, γ subunits occur as two variants, γ1 and γ2; AP-1 heterotetramers containing the former bind to a broad range of [D/E]XXXL[L/I] motifs, whereas heterotetramers containing the latter are specific for a small number of [D/E]XXXL[L/I] motifs present largely in proteins targeted to the melanosome (Kelly *et al.*, 2008; Mattera *et al.*, 2011).

A key aspect in the characterization of a basolateral sorting mechanism is the identification of the sorting adaptor involved. It is now clear that AP-1 and clathrin are key regulators of basolateral protein sorting (Deborde *et al.*, 2008; Gonzalez and Rodriguez-Boulan, 2009; Bonifacino, 2014; Nakatsu *et al.*, 2014); one study supports that AP-4 also regulates basolateral sorting (Hunziker and Fumey, 1994). The epithelium-specific variant of AP-1, AP-1B, was initially shown to mediate basolateral sorting (Fölsch *et al.*, 1999; Ohno *et al.*, 1999; Gan *et al.*, 2002; Gravotta *et al.*, 2007). AP-1A, the ubiquitous form of AP-1, possesses a different medium subunit (μ1A instead of μ1B, 85% identity) and was shown to also mediate basolateral protein sorting (Carvajal-Gonzalez *et al.*, 2012; Gravotta *et al.*, 2012). Both AP-1A and AP-1B were shown to interact with tyrosine-based basolateral sorting signals (Yxxφ) via pockets in their μ1A and μ1B subunits, structurally similar to the pocket found in the μ2 subunit of AP-2 (Carvajal-Gonzalez *et al.*, 2012). In contrast, the role of clathrin adaptors in the sorting of basolateral proteins with dileucine-based basolateral sorting signals has not been studied in depth (Table 1). A study supports a role of the clathrin machinery in the sorting of intracellular chloride channels (e.g., ClC-3–7; Stauber and Jentsch, 2010), but the role of clathrin adaptors in the sorting of plasma membrane chloride channels remains completely unknown. A decade-old study suggested that basolateral sorting of ClC-2 was mediated by AP-1B but not by AP-1A (Peña-Münzenmayer *et al.*, 2005) but did not characterize the interactions between channel and adaptors.

Here we combined in silico modeling, trafficking studies, and yeast three-hybrid assays to study in detail the mechanisms involved in the basolateral sorting of ClC-2 in MDCK cells. Our experiments demonstrate that the dileucine motif ESMI^{623}LL, different from the one previously postulated (Peña-Münzenmayer *et al.*, 2005), mediate basolateral sorting of ClC-2 and define specific interactions with the γ1–σ1 hemicomplex present in both AP-1A and AP-1B required for basolateral localization of the channel.

RESULTS

In silico molecular model of ClC-2

The human ClC-2 is a polytopic plasma membrane protein with 18 α-helices presumed to cross the bilayer and with both N- and C-terminal domains facing the cytoplasm (Dutzler *et al.*, 2002; Peña-Münzenmayer *et al.*, 2005; Feng *et al.*, 2010; Figure 1A). ClC-2 has three distinct potential dileucine motifs in its C-terminus domain:

	Surface area of residue, motif (Å^2)						Total	Norm
	–4	–3	–2	–1	0	1		
	E	**S**	**M**	**I**	**L**	**L**		
Residue	134.1	72.2	46.7	16.1	36.8	60.3	366.3	1.0
Side chain	126.5	62.1	45.5	16.1	26.7	51.5	328.4	1.0
	Q	**V**	**V**	**A**	**L**	**L**		
Residue	116.4	0.6	37.8	60.2	34.9	13.0	262.7	0.7
Side chain	107.3	0.6	34.3	40.9	34.9	13.0	230.9	0.7
	T	**I**	**F**	**S**	**L**	**L**		
Residue	52.8	13.0	0.3	26.3	101.5	62.2	256.2	0.7
Side chain	48.1	10.8	0.3	21.3	87.0	41.2	208.7	0.6

The averages of solvent accessibilities, per residue and side chain, corresponding to each motif's residue expressed in Å^2 were determined with Discovery Studio software, version 2.1 (Accelrys, San Diego, CA). Total values for each parameter measured were normalized to values corresponding to ESMI^{623}LL motif.

TABLE 2: Residue and residue side-chain solvent area in the three dileucine motifs of ClC-2.

ESMI^{623}LL and QVVA^{635}LL within CBS-1, and TIFS^{812}LL within CBS-2 (Peña-Münzenmayer *et al.*, 2005; Figure 1A). These motifs are highly conserved throughout evolution, with the exception of QVVA^{635}LL, which in birds has a methionine instead of a leucine (QVVA^{645}ML; Figure 1B).

To obtain insights into the structural environment of ESMI^{623}LL, QVVA^{635}LL and TIFS^{812}LL motifs that might help define their possible role in basolateral sorting, we built an in silico molecular model of ClC-2 based on the reported crystal structures of the eukaryote channel CmClC (Feng *et al.*, 2010) and the C-terminus segments of mammalian ClC-Ka and ClC-0 (Markovic and Dutzler, 2007). Although current crystallographic evidence for the C-terminus domain of human ClCs does not allow a complete structural characterization, the available crystal structures for the cytoplasmic C-terminal domains of ClC-0, ClC-Ka, and ClC-5 demonstrate that, within each monomer, CBS domains form dimeric Bateman modules, which in turn dimerize to form the quaternary structure of the ClC channel's cytoplasmic domain (Strange, 2011). The three-dimensional model of ClC-2 we obtained (Figure 1, C and D, and Supplemental Video S1) highlights the positions of the three dileucine motifs in ClC-2 within the context of the monomeric and dimeric configurations of the channel (Figure 1D). Surprisingly, given that TIFS^{812}LL was postulated to be a basolateral sorting signal of ClC-2, the model revealed that TIFS^{812}LL has limited structural exposure, as it is located within a region of CBS-2 sandwiched between the two monomers (Figure 1D and Supplemental Video S1). In contrast, the model predicts that ESMI^{623}LL and QVVA^{635}LL, both in the CBS1 domain, have better structural exposure. ESMI^{623}LL is integrated into a conserved sheet-loop-sheet secondary structure within CBS1 that forms an interface with CBS2 (Figure 1C), a feature common to other members of the ClC family. The calculated total solvent accessibilities of residues and residue side chains derived from this model were 1.4 times higher for ESMI^{623}LL than for to QVVA^{635}LL or TIFS^{812}LL (Table 2). Taken together, these two parameters suggest that, among the three candidate dileucine motifs, ESMI^{623}LL has the highest cytoplasmic accessibility.

The basolateral distribution of ClC-2 is abrogated by mutagenesis of ESMI^{623}LL or QVVA^{635}LL but not TIFS^{812}LL motifs

The analyses of the cytoplasmic accessibility of the three dileucine motifs in our in silico model of ClC-2 predicted that ESMI^{623}LL and to a lesser extent QVVA^{635}LL were more likely basolateral sorting signals than TIFS^{812}LL. Because this finding contradicts a previous report (Peña-Münzenmayer *et al.*, 2005), we carried out a systematic study to dissect the individual roles of these dileucine motifs in the polarized trafficking on ClC-2 in MDCK cells.

To this end, we selectively mutated the leucine pairs in each dileucine motif to alanines in the context of ClC-2 harboring a hemagglutinin (HA) epitope tag in its luminal domain (HA-ClC-2, kindly provided by Francisco Sepulveda, Centro de Estudios Científicos, Valdivia, Chile; Figure 2A) and studied the distribution of wild-type and mutant HA-ClC-2 in stably transfected MDCK cell lines. In agreement with Peña-Münzenmayer *et al.* (2005), we found that wild-type HA-ClC-2 localized preferentially to the basolateral membrane (Figure 2, B and C). In contrast with their findings, however, we found that HA-ClC-2[^{812}LL/AA] localized basolaterally in MDCK cells, exactly like wild-type (WT) HA-ClC-2 (Figure 2, B and C). Of importance, in agreement with the predictions of our structural model of ClC-2, immunolabeling of surface and total pools of HA-ClC-2[^{623}LL/AA] and HA-ClC-2[^{635}LL/AA] indicated that these proteins displayed a predominantly intracellular localization (Figure 2B), consistent with a possible sorting signal role of ESMI^{623}LL and QVVA^{635}LL. The strong intracellular retention caused by disruption of either ESMI^{623}LL or QVVA^{635}LL motifs was previously observed in nonpolarized cells (Peña-Münzenmayer *et al.*, 2005; Cornejo *et al.*, 2009).

To dissect further the possible basolateral sorting roles of ESMI^{623}LL and QVVA^{635}LL, we transplanted the cytoplasmic C-terminus domain of ClC-2 to a reporter molecule, p75 neurotrophin receptor (p75NTR), an approach that we previously used to simplify the analysis of the trafficking signals for basolateral proteins, particularly those with multiple membrane-spanning domains (Figure 2D; Le Gall *et al.*, 1997; Castorino *et al.*, 2011). Experiments carried out with these chimeras expressed in stable MDCK cell lines showed that p75-ClC-2ct (WT) and p75-ClC-2ct [^{812}LL/AA] had a normal basolateral localization, whereas p75-ClC-2ct[^{623}LL/AA] and p75-ClC-2ct[^{635}LL/AA] were predominantly localized to the apical membrane (Figure 2E). Why would these mutations cause intracellular retention of the full-size channel and apical localization of the chimeric proteins? A parsimonious interpretation is that, unlike p75NTR (Yeaman *et al.*, 1997), the full-size channel has no strong apical signals that might promote its apical expression in the absence of basolateral sorting signals (see *Discussion* for further analysis of this point).

Two major conclusions may be drawn from these experiments. First, TIFS^{812}LL does not act as a basolateral sorting signal for ClC-2.

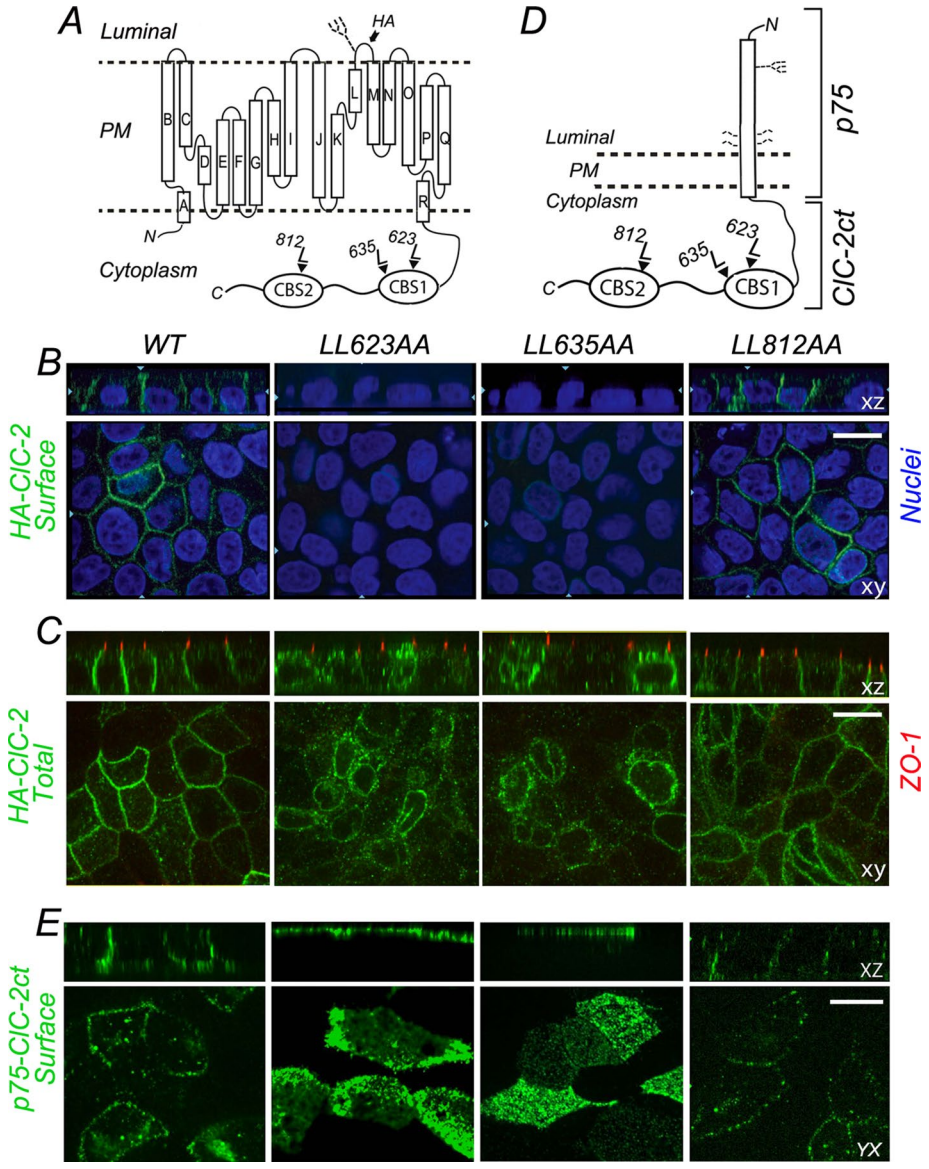

FIGURE 2: Basolateral localization of ClC-2 is disrupted by L → A mutagenesis of ESMI^{623}LL or QVVA^{635}LL. (A) Cartoon representation of HA-tagged ClC-2. The HA epitope is located in the short luminal loop between L and M α-helices; this loop contains an N-linked glycan. Note the CBS1 and CBS2 domains in the C-terminus that house the three dileucine motifs. (B) Stable MDCK cell lines expressing WT or mutant HA-ClC-2 with alanine replacements of dileucine pairs for each individual dileucine motif, HA-ClC-2[^{623}LL/AA], HA-ClC-2[^{635}LL/AA], and HA-ClC-2[^{812}LL/AA]. Cells were polarized after 4 d and cultured on Transwell filters and immunolabeled with HA antibody before permeabilization to decorate surface ClC-2 (green). Note the basolateral localization of HA-ClC-2[WT] and HA-ClC-2[^{812}LL/AA]; in contrast, HA-ClC-2[^{623}LL/AA] and HA-ClC-2[^{635}LL/AA] are not expressed at the cell surface. (C) The same cell lines shown in B were decorated with HA antibodies after cell permeabilization; tight junctions are labeled with anti-ZO1 (red). Note the intracellular accumulation of HA-ClC-2[^{623}LL/AA] and HA-ClC-2[^{635}LL/AA] mutants. (D) Cartoon representation of p75-ClC-2ct chimera constructed by fusing the luminal, transmembrane, and eight cytoplasmic residues of p75 with the entire C-terminus domain (347 amino acids) of ClC-2. The single N-linked glycan and four O-linked glycans of p75 are displayed. (E) Stable MDCK cells lines expressing WT p75-ClC-2ct or the dileucine mutants p75-ClC-2ct[^{623}LL/AA], p75-ClC-2ct[^{635}LL/AA], and p75-ClC-2ct[^{812}LL/AA]. Cells were cultured for 4 d on Transwell filters, fixed without permeabilization, and immunolabeled with mouse antibodies to the ectodomain of p75 (green) to visualize the surface distribution of the chimeric proteins. Note the basolateral localization of WT p75-ClC-2ct and p75-ClC-2ct[^{812}LL/AA] and the apical redistribution of p75-ClC-2ct[^{623}LL/AA] and p75-ClC-2ct[^{635}LL/AA].

Second, ESMI^{623}LL and QVVA^{635}L are involved in the basolateral sorting of ClC-2 but are not able to act as independent basolateral signals, as they do not show evidence of redundancy. We hypothesize that only one of these two motifs is the authentic basolateral sorting signal, whereas the other one plays a structural role in CBS1 that supports the sorting signal function of the other motif. The following experiments were designed to test this hypothesis.

ESMI^{623}LL is the authentic basolateral sorting signal of ClC-2

Collectively the information provided by the in silico model of ClC-2 and the foregoing mutagenesis experiments suggested that ESMI^{623}LL and QVVA^{635}LL contribute to the basolateral sorting signal of ClC-2. To collect additional evidence that would allow us to determine which motif functions as the authentic basolateral signal of ClC-2, we carried out mutagenesis of individual residues in each of the two motifs to dissect their individual contributions to the basolateral localization of ClC-2 after transient expression of the mutant proteins into polarized MDCK cells. Cell surface and total HA-ClC-2 were determined by sequentially immunolabeling the luminal HA epitope in intact cells and after cell permeabilization with two different species of anti-HA antibodies (Figure 3A). Representative images of confocal sections derived from these experiments are shown in Figure 3B. Data obtained from quantification of these experiments were expressed as fractional distribution of surface versus intracellular HA-ClC-2 (Figure 3C) and analyzed for statistical significance using analysis of variance (ANOVA) and Bonferroni's *t* test corrections (Figure 3C and Supplemental Table S1).

We observed that HA-ClC-2 localized predominantly to the plasma membrane (0.80 ± 0.03), with a small fraction retained intracellularly (0.20 ± 0.03; Figure 3, B and C). In contrast, most of HA-ClC-2[^{623}L/A] was localized intracellularly (0.72 ± 0.02), with only a small fraction at the cell surface (0.28 ± 0.02), representing a 64% reduction and a 350% increase in the surface and intracellular distributions, respectively (Figure 3, B and C, and statistical analyses in Supplemental Table S1). Of importance, the localization of HA-ClC-2[^{624}L/A] was also significantly altered compared with that of HA-ClC-2, with approximately equal surface and intracellular pools (0.52 ± 0.02 and 0.48 ± 0.02, representing a 35% reduction and a 236% increase, respectively; Figure 3, B and C; see statistical analyses in

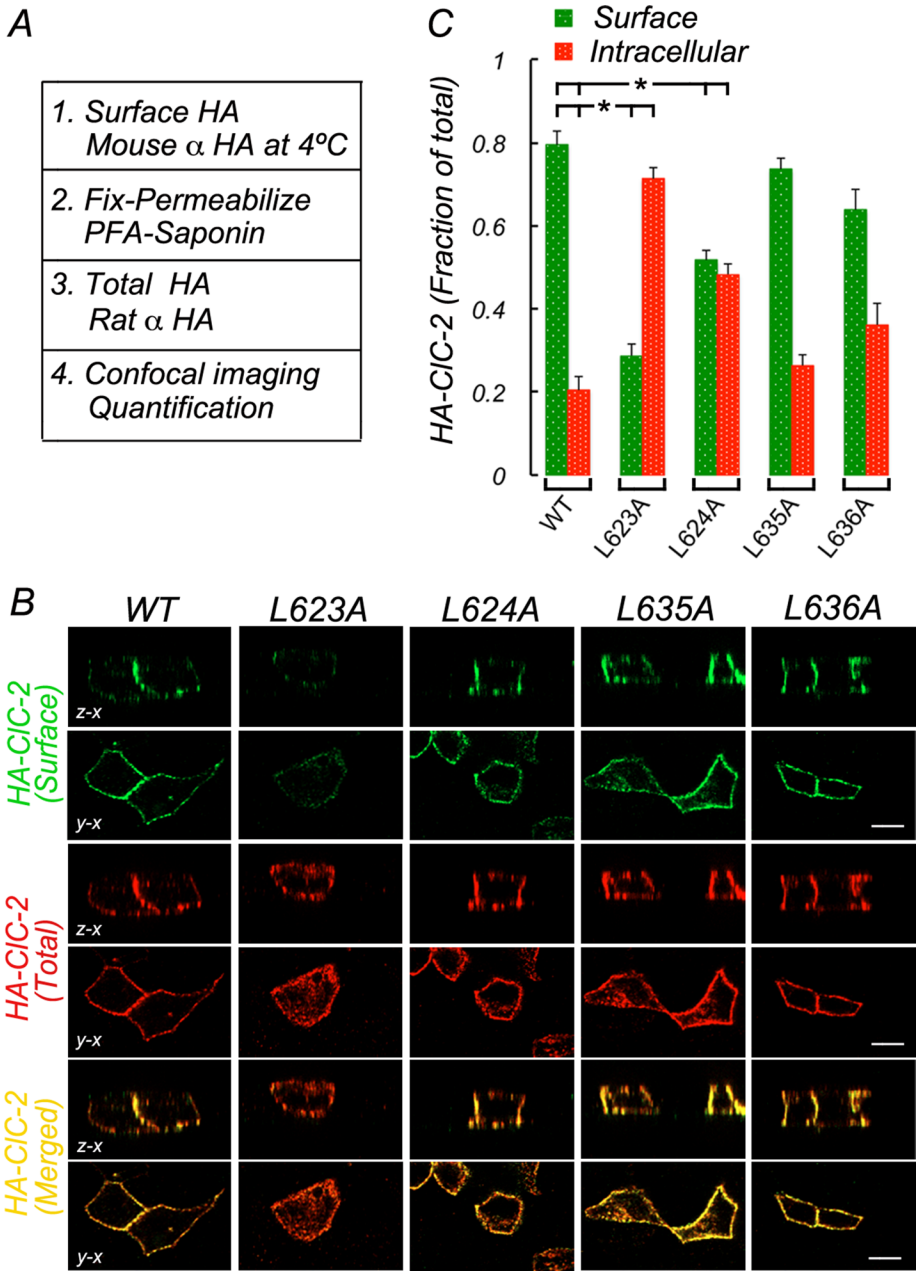

FIGURE 3: ESMI^{623}LL motif controls basolateral localization of HA-ClC-2. Wild-type and mutant HA-CLC-2 with single leucine residues replaced by alanine in ESMI^{623}LL or QVVA^{635}LL were transiently expressed in MDCK cells allowed to polarize for 4 d in culture. (A) Procedure to sequentially immunolabel HA-ClC-2 before and after saponin permeabilization with mouse and rat antibodies to luminal HA, respectively (see *Materials and Methods* for details). (B) Surface (green) and total (red) HA-ClC-2 in fully polarized cells. Note that wild-type HA-ClC-2[WT] is restricted to the basolateral membrane, whereas HA-ClC-2 [^{623}L/A] is depleted from the cell surface and accumulated intracellularly. (C) Bars represent fractions of surface and intracellular HA-ClC-2 calculated from confocal images (see *Materials and Methods* for details). Statistically significant reductions in surface localization of HA-ClC-2 [^{623}L/A] and HA-ClC-2 [^{624}L/A] are indicated. No significant changes in HA-ClC-2 [^{635}L/A] or HA-ClC-2 [^{636}L/A] were observed. Detailed statistical analysis is shown in Supplemental Table S1. Bar, 12 μm.

Supplemental Table S1). Equivalent analysis of the QVVA^{635}LL motif indicated that the single mutants HA-ClC2[^{635}L/A] and HA-ClC2 [^{636}L/A] did not display significant intracellular retention (Figure 3, B and C, and Supplemental Table S1). Thus, because individual leucine mutagenesis of ESMI^{623}LL disrupted basolateral localization of ClC-2, we conclude that QVVA^{635}LL cannot mediate basolateral sorting as an independent basolateral signal. Furthermore, leucine mutagenesis of QVVA^{635}LL did not cause missorting of ClC-2, which is consistent with the idea that ESMI^{623}LL is the only basolateral signal of ClC-2.

To complete the characterization of ESMI^{623}LL as a basolateral sorting signal, we carried out alanine substitutions of the remaining residues and performed the localization assay described. The mutants generated, HA-ClC-2[^{619}E/A], HA-ClC-2[^{620}S/A], and HA-ClC-2[^{622}I/A], were expressed in MDCK cells and their distribution quantified essentially as described in Figure 3A (Supplemental Figure S2). All mutants displayed similar surface and intracellular distributions as wild-type HA-ClC-2 (Supplemental Figure S2, B and C; see statistical analyses in Supplemental Table S3), indicating that, unlike ^{623}L and ^{624}L, the respective mutated residues were not required for basolateral sorting of ClC-2. Taken together, these experiments further strengthen the hypothesis that ESMI^{623}LL is the authentic basolateral sorting signal of ClC-2.

We validated our quantitative imaging results by using an alternative biochemical approach. We generated a lentivirus panel encoding all of the individual leucine–alanine replacements and quantified apical, basolateral and intracellular distributions of HA-ClC-2 mutants in polarized infected MDCK cells using a previously described surface biotinylation avidin shift (SBAS) assay (Gravotta *et al.*, 2012; Supplemental Figure S4). Overall these experiments were in agreement with the observation in transient transfected cells, as they supported a signaling role for ESMI^{623}LL in the basolateral sorting of CLC-2 (Supplemental Tables S1 and S5).

Because HA-ClC-2[^{623}L/A] failed to reach the surface and accumulated intracellularly, we quantified the accumulation of this mutant at intracellular transit compartments. Colocalization analysis using the *trans*-Golgi network (TGN) marker TGN38 and the endosomal marker transferrin receptor revealed a moderate steady-state accumulation of the mutant at the level of the TGN (Supplemental Table S6).

Clathrin adaptors AP-1A and AP-1B mediate basolateral sorting of ClC-2

Next we carried out experiments to identify the machinery that mediates basolateral trafficking of ClC-2. Both variants of the clathrin-adaptor AP-1, AP-1B (Fölsch *et al.*, 1999; Ohno *et al.*, 1999) and AP-1A (Carvajal-Gonzalez *et al.*, 2012; Gravotta *et al.*, 2012), have been implicated in basolateral sorting. These tetrameric adaptors share three subunits (β1, σ1, and γ1) and have different, albeit highly homologous (85%), medium subunits

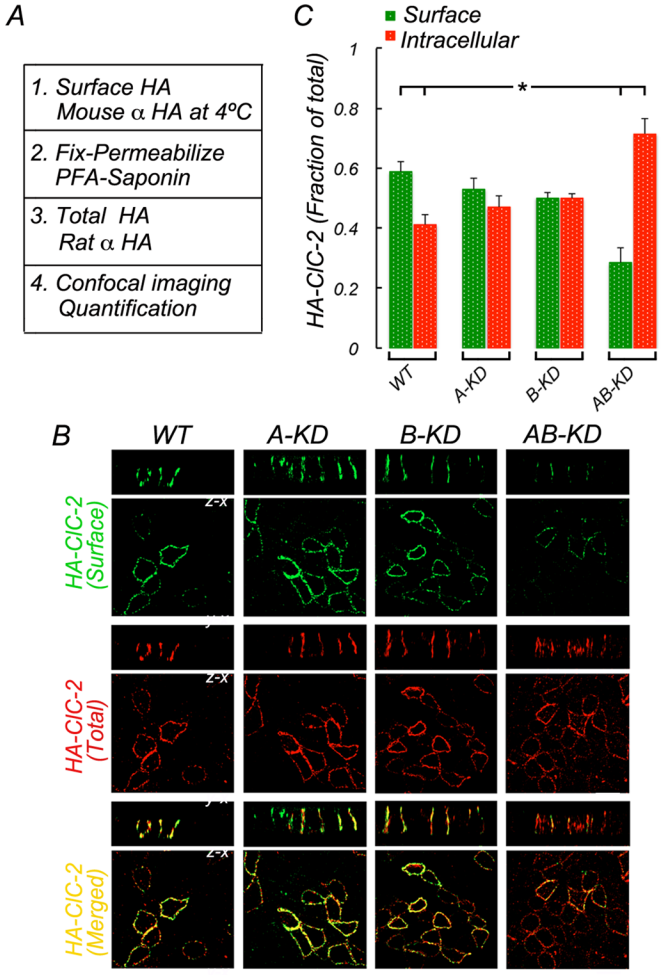

FIGURE 4: Double knockdown of clathrin adaptors AP-1A and AP-1B inhibits surface expression of full-length ClC-2. MDCK cells, WT or depleted of μ1A (A-KD), μ1B (B-KD), or both (AB-KD) with specific siRNAs (see *Materials and Methods*). Knocked-down cells were transiently transfected with HA-ClC-2 (see *Materials and Methods*). (A) Procedure to sequentially immunolabel HA epitope in intact and permeabilized cells, as described in Figure 3A. (B) Surface (green) and total (red) immunolabeling of HA-ClC-2 in fully polarized cells. Note the reduction of surface levels of HA-ClC-2 and consequent increase of its intracellular levels in AB-KD cells. (C) Bars represent surface and intracellular fractions of HA-ClC-2, calculated from confocal images (see *Materials and Methods* for details). Statistically significant reduction in surface HA-ClC-2 and increase in intracellular HA-ClC-2 was found only in AB-KD cells. Detailed statistical analysis is shown in Supplemental Table S7. Bar, 15 μm.

(μ1A and μ1B). Stable MDCK cells expressing HA-ClC-2 were treated with small interfering RNAs (siRNAs) against μ1A (A-KD), μ1B (B-KD), both μ1A and μ1B (AB-KD), or luciferase (control, WT) and analyzed 10 d later; the siRNAs were previously characterized (Carvajal-Gonzalez *et al.*, 2012; Gravotta *et al.*, 2012; Figure 4A). In singly silenced A-KD and B-KD cells, HA-ClC-2 localized predominantly to the basolateral membrane, a distribution similar to that displayed by WT MDCK cells. In contrast, MDCK cells in which both μ1A and μ1B were knocked down (AB-KD) exhibited a drastic reduction (>50%) in surface localization and a corresponding increment (190%) in intracellular localization of the channel compared with WT cells (Figure 4, B and C; statistical analysis in Supplemental Table S7).

We further tested the roles of AP-1A and AP-1B in the sorting of ClC-2 in the context of the p75-ClC-2ct chimera (Figure 5). Stable MDCK cell lines expressing p75-ClC-2ct were subjected to silencing of μ1A and μ1B, as described, and immunolabeled as described in Figure 3A using two different species of anti-p75 antibody to detect surface and total pool of chimeras (Figure 5A). In WT cells, p75-ClC-2ct was found preferentially at the basolateral membrane (0.43 ± 0.02), with a minor proportion at the apical membrane (0.02 ± 0.0062; Figure 5, B and C; statistical analyses in Supplemental Table S8). Similar basolateral distributions were determined for A-KD (0.52 ± 0.02) and B-KD (0.48 ± 0.01) cells (Figure 5, B and C; statistical analyses in Supplemental Table S8). In contrast, AB-KD MDCK cells shifted a substantial fraction of p75-ClC-2ct toward the apical membrane (0.16 ± 0.02), significantly larger than that determined for WT cells (0.02 ± 0.006), increasing >10-fold the AP/BL ratio from 0.05 in WT MDCK cells to 0.6 in AB-KD MDCK cells (Figure 5, B and C; statistical analyses in Supplemental Table S8). Of importance, the intracellular fraction of ClC-2 remained the same in WT, A-KD, B-KD, and AB-KD MDCK cells, suggesting that the presence of strong apical signals in p75 was sufficient to prevent intracellular accumulation of the chimeric proteins upon removal of the adaptors that recognize ClC-2's basolateral signal (Figure 5D).

Taken together, these experiments indicated that the presence of either AP-1A or AP-1B variants of AP-1 is sufficient to generate and maintain a basolateral distribution of ClC-2.

ESMI^{623}LL but not TIFS^{812}LL interacts with γ1–σ1A hemicomplex of AP-1

Collectively the evidence discussed so far reveals that ClC-2 uses the dileucine motif ESMI^{623}LL or QVVA^{635}LL as a basolateral sorting signal and requires either AP-1A or AP-1B for basolateral localization in polarized MDCK cells. If these conclusions are correct, we might expect to detect direct interactions between one of the two dileucine motifs and both adaptors using a yeast three-hybrid (Y3H) assay. To this end, we carried out Y3H assays using the 347–amino acid C-terminal cytoplasmic domain of ClC-2 and the γ1–σ1A hemicomplex present in both AP-1A and AP-1B. As positive control, we used the HIV Nef (NLA4-3 variant) protein, which displays a canonical, dileucine motif (ENTSLL) that mediates selective interaction with γ1–σ1A (AP-1) and δ–σ3A (AP-3) but not with α–σ2 (AP-2) (Janvier *et al.*, 2003; Doray *et al.*, 2007). Qualitative and quantitative forms of the Y3H assay (plate and liquid growth, respectively; see details in *Materials and Methods*) revealed that wild-type ClC-2ct interacted specifically with the γ1–σ1A hemicomplex, albeit with less avidity than Nef B (Figure 6, A and B). Of importance, alanine substitution of both leucine residues in TIFS^{812}LL had no effect on this Y3H interaction; in contrast, double-alanine substitution in either ESMI^{623}LL or QVVA^{635}LL abrogated the interaction with γ1–σ1A (Figure 6, A and B). These observations are in close agreement with the alanine mutagenesis/trafficking experiments described in Figure 2, which suggested that either ESMI^{623}LL or QVVA^{635}LL, but not TIFS^{812}LL, was a candidate basolateral sorting signal for the channel. Furthermore, they agree with our hypothesis that these two motifs do not behave as independent basolateral sorting signals for the channel.

To obtain additional evidence for the sorting signal activity of ESMI^{623}LL or QVVA^{635}LL, we studied the Y3H interaction between the ClC-2 C-terminal domain with single-alanine substitutions in ESMI^{623}LL or QVVA^{635}LL and the γ1–σ1A hemicomplex. Strikingly, these experiments revealed that both mutations in ESMI^{623}LL, L623A, and L624A disrupted the interaction with γ1–σ1A (Figure 6, C and D), compatible with an authentic basolateral signal role for this dileucine motif. In contrast, mutation of only one of the leucines in QVVA^{635}LL,

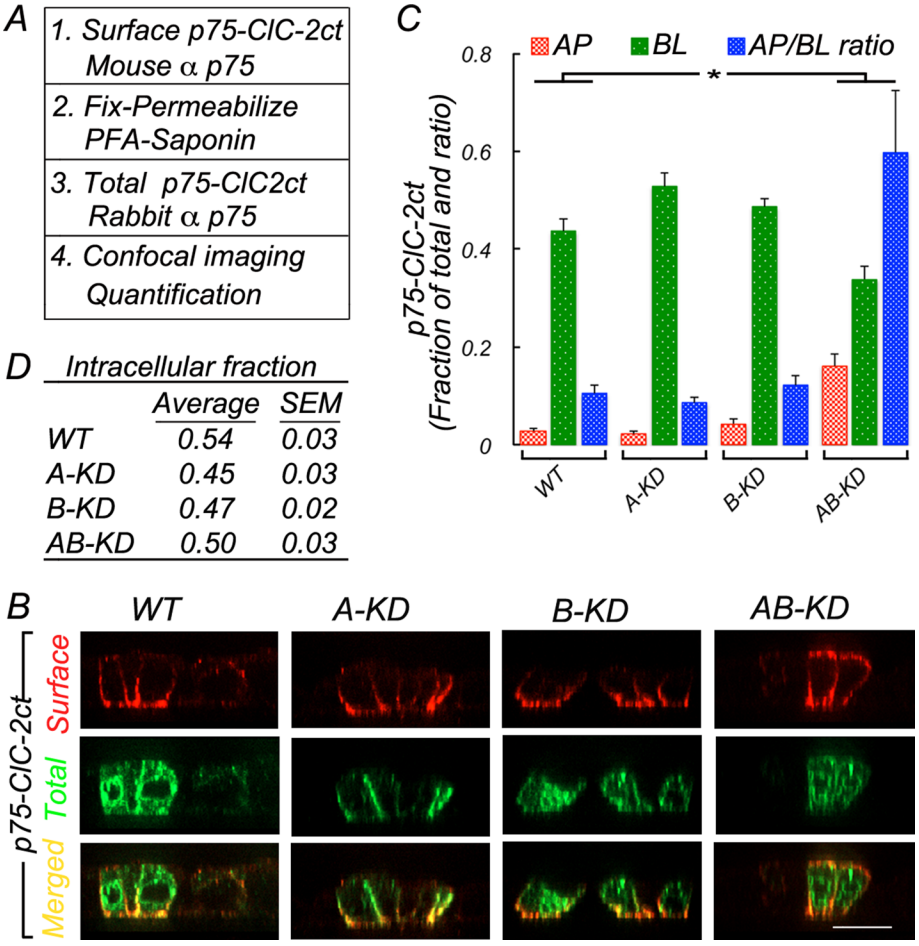

FIGURE 5: Double knockdown of clathrin adaptors AP-1A and AP-1B promote apical missorting of the p75-ClC-2ct chimera. MDCK cells permanently expressing the p75-ClC-2ct chimera were silenced for μ1A (A-KD), μ1B (B-KD), or both (AB-KD) with specific siRNAs (see *Materials and Methods*) and processed for immunofluorescence after 4 d in culture. (A) Surface and total p75-ClC-2ct sequentially immunolabeled before and after permeabilization with mouse and rabbit anti-p75 antibodies, respectively (see *Materials and Methods* for details). (B) Note that whereas WT, A-KD, and B-KD MDCK cells display basolateral localization of p75-ClC-2ct, AB-KD MDCK cells display partial apical redistribution of the chimera. (C) Bars represent fractions of apical (AP) and basolateral (BL) p75-ClC-2ct, calculated from confocal images (see *Materials and Methods* for details) and the A/BL ratio for each experimental condition. (D) Average values of intracellular fractions were calculated from confocal images (see *Materials and Methods*). Detailed statistical analysis is shown in Supplemental Table S8. Bar, 20 μm.

L636A, or L636S but not of the other one, L635A or L635S, inhibited the Y3H interaction of ClC-2ct with the γ1–σ1A hemicomplex, inconsistent with the expected behavior of an authentic dileucine sorting motif. A similar strategy to test the interaction of the remaining residues in both dileucine motifs revealed no or minimal roles of the residues at positions –4 (^{619}E or ^{631}Q), –2, and –1 (Figure 6, E and G).

In summary, in close agreement with the trafficking experiments described earlier that prioritized ESMI^{623}LL over QVVA^{635}LL as a candidate basolateral signal, the Y3H experiments in this section indicate that the interaction of ESMI^{623}LL with the γ1–σ1A complex is more typical of a cognate dileucine motif than that of QVVA^{635}LL.

Mutations in the highly conserved γ1–σ1A pocket of AP-1 disrupt interaction with the basolateral signal of ClC-2

Crystallographic analysis of the α–σ2 hemicomplex of AP-2 and peptides containing the dileucine motif identified residues in the hydrophobic pocket–for example, ^{65}L, ^{88}V, and ^{98}V in the σ2 subunit—that accommodate the dileucine motif (Kelly *et al.*, 2008). More recently, equivalent residues in the subunit σ1 of AP-1, ^{63}A and ^{88}V, have been found to interact with Nef's ENTSLL (Mattera *et al.*, 2011). On the basis of these previous observations, we modeled in silico the interaction between the basolateral signal of ClC-2, ESMI^{623}LL, and AP-1's hemicomplex γ1–σ1A. The model suggested important interactions with key conserved residues in σ1A. In particular, it suggested that ^{623}L in ClC-2 binds to a hydrophobic pocket constituted by the side chains of residues ^{63}A, ^{65}L, ^{88}V, and ^{98}V in σ1A (Figure 7A). An additional hydrophobic interaction (H bonds) may occur between the nitrogen amide of ^{623}L in ClC-2 and a carboxyl group of ^{98}V in σ1A. A second hydrophobic pocket, generated by the side chains of ^{62}Y and ^{88}V in σ1A, is predicted to accommodate the side chain of ^{624}L in ClC-2. The model suggests hydrogen bonding between side chains of ^{621}M in ClC-2 and ^{63}A in σ1A, between the side chain of ^{64}S in σ1A and ^{618}P in ClC-2, and between the carboxyl group of ^{619}E in ClC-2 and backbone nitrogens of ^{100}E and ^{101}L in σ1A. It also suggests that the carboxyl group of ^{619}E in ClC-2 establishes extensive polar interactions with side chains of ^{15}R in σ1A and ^{15}R in γ1 (Figure 7B).

To attempt to validate these in silico predictions, we evaluated experimentally the effect of three point mutations (^{65}L/S, ^{88}V/D, and ^{98}V/S) in σ1A on the interaction with ClC-2ct by Y3H assays (Figure 7, C and D). We found that ^{65}L/S and ^{88}V/D mutations strongly abrogated the interaction.

Finally, we examined whether we could detect any association in vivo between intact tetrameric AP-1 and ClC-2. MDCK cells stably expressing ClC-2-GFP were subjected to immunoprecipitation of detergent-solubilized membranes using an anti–γ-adaptin antibody. Western blotting analysis revealed that the immunoprecipitate contained ClC-2–green fluorescent protein (GFP), indicating the existence of a complex between ClC-2-GFP and intact tetrameric AP-1.

DISCUSSION

A major incentive for these studies was the fact that, in spite of their growing relevance to a variety of physiological processes and human diseases, chloride channels remain vastly unexplored in terms of the mechanisms that control their subcellular distribution. We decided to focus on ClC-2 because of its physiological importance as a regulator of fluid transport in a variety of epithelia, including blood–retinal and blood–testis barriers (Bosl *et al.*, 2001; Nehrke *et al.*, 2002; Edwards *et al.*, 2010). Furthermore, ClC-2 provided an opportunity to study the sorting machinery involved in the trafficking of a basolateral protein with a dileucine sorting signal: although about a dozen proteins were shown to be sorted basolaterally in epithelial cells through dileucine motifs (Table 1), the molecules

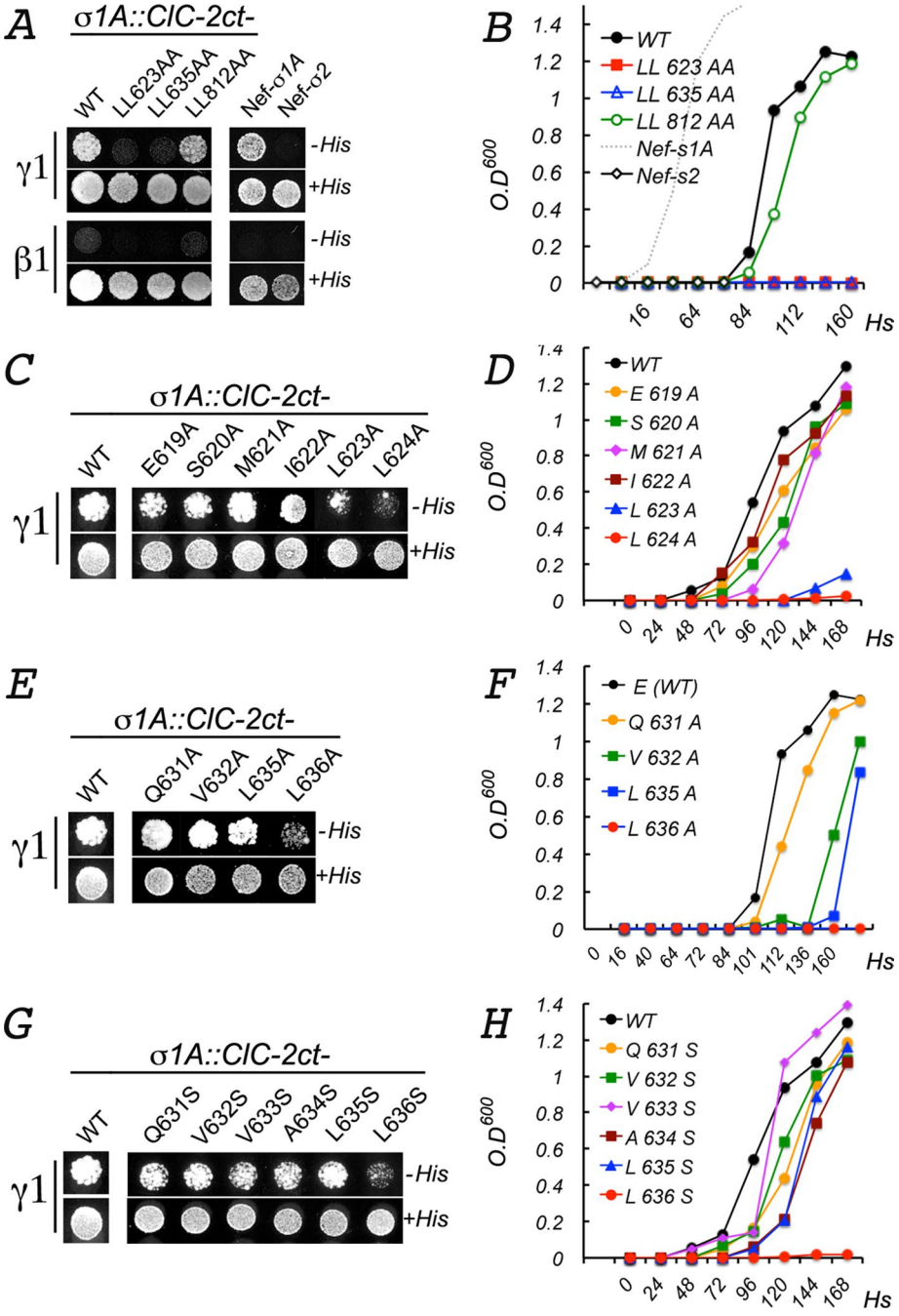

FIGURE 6: Yeast three-hybrid analysis of the interaction between ClC-2ct and AP-1. The full C-terminus domain (347 amino acids) of ClC-2 (CLC-2ct) and the human σ1A subunit of AP-1 were cloned into different cloning sites of the pBridge vector. The γ1 or β1 subunit was cloned into the pGADT7 vector (see *Materials and Methods* for details). Growth of cotransformed yeast, reflecting bait/prey interactions, was monitored on plates (A, C, E, G) for 4–6 d or in liquid medium (B, D, F, H) for 0–7 d in the presence or absence of histidine. Quantification of the interaction in liquid medium (B, D, F, H) was determined by spectrometry at 600 nm. (A, B) Wild-type ClC-2ct specifically interacted with the γ1-σ1A hemicomplex, although less robustly than Nef (compare black line with dotted gray line in B). Note that ClC-2ct[^{812}LL/AA] interacted with γ1-σ1A (green line) as robustly as WT ClC-2ct (black line). In contrast, ClC-2ct[^{623}LL/AA] and ClC-2ct[^{635}LL/AA] failed to interact with γ1-σ1A. (C, D) Single alanine substitutions in ESMI^{623}LL. The interaction with γ1-σ1A was blocked only by substitutions ^{623}L/A and ^{624}L/A. Note that alanine substitution of the glutamic acid at –4 position did not inhibit the interaction. (E, F) Single alanine substitutions in QVVA^{635}LL. The interaction with γ1-σ1A was abolished only by ^{636}L/A. (G, H) Single serine substitutions QVVA^{635}LL. The interaction with γ1-σ1A was abolished only by ^{636}L/S.

involved in their polarized distribution have not been characterized. A decade-old comparative study of normal and ClC-2–knockout mice conclusively demonstrated the basolateral localization of this channel in intestinal mucosal epithelia and suggested that a dileucine motif in its cytoplasmic domain and the clathrin adaptor AP-1B were involved in its sorting (Peña-Münzenmayer *et al.*, 2005). Because ClC-2 has three dileucine motifs, we generated an in silico model of ClC-2 to assess their potential basolateral sorting role (Figure 1). Surprisingly, our model clearly indicated that TIFS^{812}LL, postulated to be the channel's basolateral sorting signal, was hidden in a dimerization region of the channel; thus, because dimerization likely occurs early during biogenesis (Jentsch, 2002), this motif would not be available to interact with the sorting machinery during trafficking to the cell surface. In contrast, ESMI^{623}LL and QVVA^{635}LL, the two other dileucine motifs, were exposed to the cytoplasm, with ESMI^{623}LL having higher residue and side-chain solvent accessibility than QVVA^{635}LL (Figure 1 and Table 2), suggesting that one or both of them might perform as basolateral signals for ClC-2. These observations drove us to dissect the role of the three dileucine motifs in the basolateral sorting of ClC-2.

To characterize initially the possible sorting role of each dileucine motif, we carried out double-alanine substitution of their leucine pairs (Figure 2). These studies confirmed the prediction of our in silico model regarding TIFS^{812}LL, as mutation of its dileucine pair did not disrupt the basolateral localization of HA-ClC-2. It is not clear why our results differ from those by Peña-Münzenmayer *et al.* (2005) in this regard. Furthermore, our studies also clearly showed that double-leucine replacement in either ESMI^{623}LL or QVVA^{635}LL in the context of the full-length channel caused strong intracellular retention of ClC-2 (Figure 2, B and C). Furthermore, experiments with chimeras of the extracellular and transmembrane domains of p75 and the C-terminal domain of ClC-2 (p75-CLC-2ct) showed that wild-type p75-CLC-2ct localized to the basolateral PM of MDCK cells, whereas double-leucine substitution of either ESMI^{623}LL or QVVA^{635}LL resulted in transport of the mutant proteins to the apical surface rather than intracellular retention (Figure 5). The mislocalization of the mutant full-size and chimeric channel reflects the absence of functional signals to promote trafficking from the sorting compartment to the cell surface. Whereas the retention of mutant ClC-2 reflects the

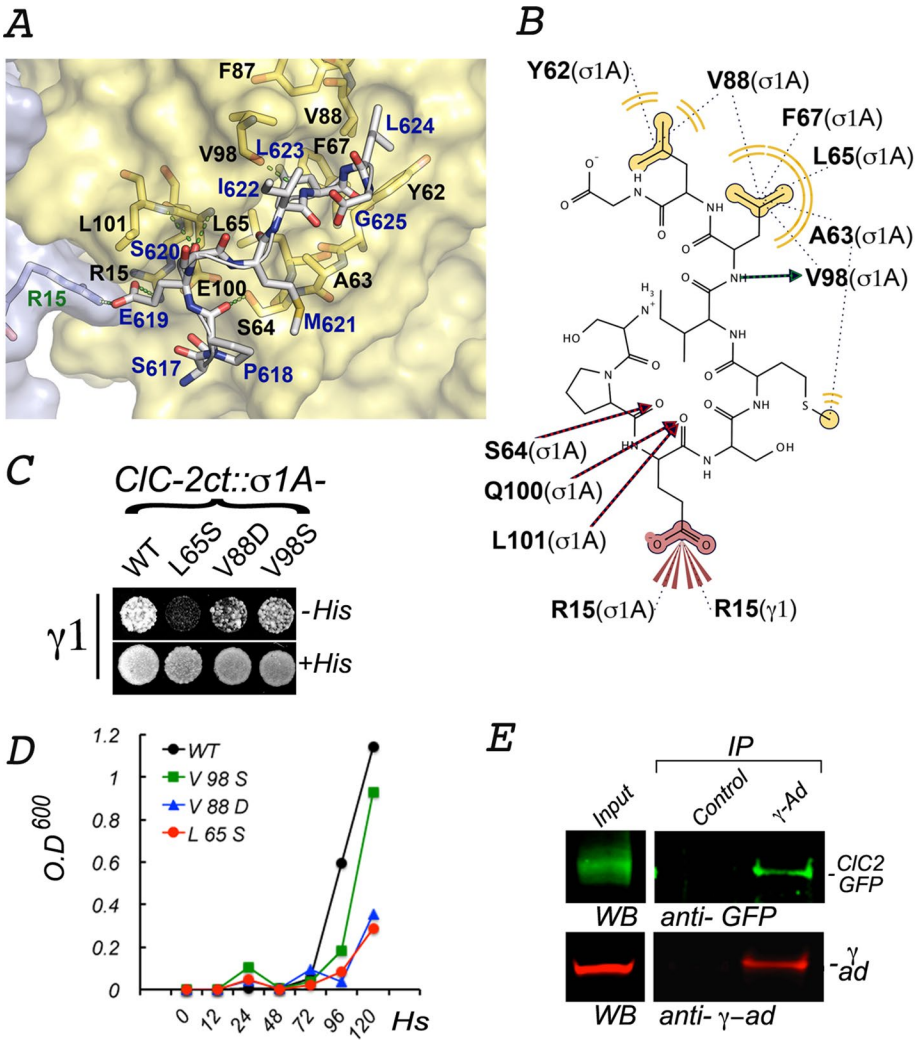

FIGURE 7: Interactions between ESMI^{623}LL and a conserved pocket in γ1-σ1A. (A) In silico model of the interaction between ESMI^{623}LL and γ1-σ1A. The structure of the γ1-σ1A pocket of AP-1 that interacts with ESMI^{623}LL was modeled from the crystal structure of the corresponding pocket in the α–σ2 hemicomplex of AP-2 (2JKR) (see *Materials and Methods*). The names of the key pocket residues in the surface-rendered yellow representation of σ1A (black font) and gray representation of γ1 (green font) are shown as yellow and orange sticks. The residues in ESMI^{623}LL (blue font), superimposed on the pocket, are shown in gray sticks with oxygen atoms in red and nitrogen atoms in blue. (B) Two-dimensional representation of the interaction of ESMI^{623}LL with the γ1-σ1A pocket. The model shows the leucine residues in ESMI^{623}LL coordinating with σ1 hydrophobic residues (^{62}Y, ^{65}L, ^{67}Phe, ^{88}V, and ^{98}V), whereas the negatively charged residue ^{619}E at –4 position coordinates with positively charged residues ^{15}R in σ1 and ^{15}R in γ1. (C, D) Yeast three-hybrid assay shows that interaction of CLC-2ct with γ1-σ1A is inhibited by mutations of two of the residues predicted to be involved in the interaction (^{65}L, ^{88}V). (E) Coimmunoprecipitation of ClC-2-GFP and AP-1. On immunoprecipitation with mouse γ-adaptin antibodies, the presence of both ClC-2-GFP and γ-adaptin in the precipitate is observed by Western blot.

lack of strong apical signals in its extracellular domain (just one N-glycan in the extracellular loop between the L and M α-helices; Figure 2A), the apical localization of the mutant chimeric channel is driven by strong apical sorting signals, that is, N- and O-glycans in the extracellular domain of p75 (Yeaman *et al.*, 1997). In agreement with this interpretation, it has been shown that disease-causing mutations of a signal patch in the potassium channel Kir 2.1 required for binding AP-1 block export of the channel from the Golgi apparatus (Ma *et al.*, 2011). Taken together, these experiments suggested that ESMI^{623}LL and QVVA^{635}LL are required for the basolateral sorting of ClC-2, albeit not as independent and redundant basolateral signals. They also suggested that double-alanine mutagenesis has insufficient resolution to distinguish between sorting and structural roles of each individual motif.

Both ESMI^{623}LL and QVVA^{635}LL are present within the highly structured CBS-1 domain of the cytoplasmic tail of ClC-2. Hence, to determine which one of these dileucine motifs behaves as a dileucine-based basolateral sorting signal, we used a classical and less intrusive strategy to study their sorting role—single-alanine mutagenesis of all amino acid residues in each motif within the context of the full-size channel. Strikingly, mutation of individual leucines in ESMI^{623}LL reduced basolateral localization and increased intracellular retention of the mutant channel, whereas mutagenesis of the –3, –2, and –1 (S, M, and I) did not affect basolateral localization of the channel (Supplemental Figure S2). Mutagenesis of acidic residue ^{619}E did not cause missorting of the channel, in agreement with the inconsistent sorting requirement for acidic residues in position –4 in dileucine motifs (Table 1; Hunziker and Fumey, 1994; Janvier *et al.*, 2003; Doumanov *et al.*, 2006; Mattera *et al.*, 2011). In contrast, replacement of each individual leucine in QVVA^{635}LL had no significant effect on the channel's distribution. These experiments strongly suggest that ESMI^{623}LL is the authentic basolateral sorting signal of ClC-2.

Because both variants of the clathrin adaptor AP-1, AP-1A and AP-1B, have been implicated in basolateral sorting, we then used single or combined knockdown of AP-1A and AP-1B in MDCK cells, an approach we recently reported (Carvajal-Gonzalez *et al.*, 2012; Gravotta *et al.*, 2012), to study their role in basolateral sorting of ClC-2. Individual knockdown of either AP-1A or AP-1B did not disrupt the basolateral localization of ClC-2. In contrast, knockdown of both AP-1A and AP-1B resulted in intracellular retention of full- length ClC-2 and apical relocalization of the p75-ClC-2ct chimera (Figures 4 and 5). These results differ from gain-of-function experiments reported in AP-1B–deficient LLC-PK1 cells, showing that overexpression of the clathrin adaptor AP-1B but not of AP-1A corrects the nonpolarized distribution of ClC-2. Because AP-1A is expressed endogenously by LLC-PK1 cells, those experiments suggested that AP-1B but not AP-1A is necessary for basolateral expression of ClC-2 (Peña-Münzenmayer *et al.*, 2005). In contrast, our results demonstrate that expression of either AP-1A or AP-1B in MDCK cells is sufficient to confer basolateral localization to ClC-2.

If both AP-1A and AP-1B participate in the sorting of ClC-2, it should be possible to demonstrate that these adaptors interact

specifically with this channel's basolateral sorting signal. Y3H studies show that [D/E]XXXL[L/I] dileucine motifs interact with γ–σ1, α–σ2, and δ–σ3 hemicomplexes in AP-1, AP-2, and AP-3, respectively; these interactions mediate the known biological functions of these adaptors—for example, Nef-mediated down-regulation of CD4 and lysosomal targeting of LIMP-II. A study by Mattera *et al.* (2011) further showed that the interaction of dileucine motifs with AP-1 also depends on the combinatorial assembly of various γ and σ1 isoforms—for example, γ1 and γ2, and σ1A, σ1B, and σ1C. For example, Nef and LIMP-II interacted with AP-1 hemicomplexes containing γ1 and σ1A, B or C, whereas tyrosinase interacted preferentially with γ2–σ1A and γ2–σ1B hemicomplexes. Our studies demonstrated that the cytoplasmic domain of ClC-2 interacts well with γ1–σ1A, present in both AP-1A and AP-1B, as expected from our trafficking studies in MDCK cells silenced for both adaptors. This interaction was disrupted by alanine substitution ^{623}L/A but was unaffected by ^{635}L/A, strengthening the conclusion that ESMI^{623}LL controls the basolateral sorting of ClC-2 through direct interactions with the γ–σ1A hemicomplex present in both AP-1A and AP-1B. Furthermore, on the basis of crystallographic and biochemical studies that characterized the residues in the γ–σ1 and α–σ2 pockets that interact with the dileucine motifs (Janvier *et al.*, 2003; Kelly *et al.*, 2008; Mattera *et al.*, 2011), we carried out in silico modeling experiments that suggested key interactions between ESMI^{623}LL and conserved residues in σ1A and confirmed these in silico predictions with Y3H assays.

In summary, our experiments characterize in detail the role of AP-1 in the sorting of a basolateral plasma membrane protein with a dileucine-based basolateral sorting signal in a model epithelial cell (MDCK). Although in this case, AP-1A and AP-1B appear to play equivalent roles in the sorting of ClC-2, other work suggests that for certain basolateral proteins, particularly those with fast recycling kinetics, AP-1A cannot fully replace AP-1B (Gonzalez and Rodriguez-Boulan, 2009). Hence current work in our laboratory aims to explore how exactly AP-1A mediates basolateral sorting in epithelial tissues that lack AP-1B, such as RPE (Diaz *et al.*, 2009) and kidney proximal tubule (Schreiner *et al.*, 2010). In addition, because there is significant evidence that ClC-2 may have an apical distribution in certain epithelial tissues, an important goal for the future is to study the possible role of ClC-2–interacting proteins, such as GlialCAM and cereblon (Hohberger and Enz, 2009; Jeworutzki *et al.*, 2012), as potential accessory subunits of ClC-2 that regulate its trafficking in order to accommodate local tissue requirements. In addition, because ClC-2 displays a large intracellular pool and endocytic signals (Cornejo *et al.*, 2009), it will be important in the future to study how postendocytic recycling contributes to the surface polarity of this channel.

MATERIALS AND METHODS

Plasmids and mutagenesis

Vectors (pCR3.1) encoding ClC-2-GFP and HA-ClC-2 were kindly provided by Francisco Sepulveda (Centro de Estudios Cientificos [CECs], Valdivia, Chile; Peña-Münzenmayer *et al.*, 2005). The p75-ClC-2ct chimera was constructed by amplification of C-terminus fragment of human ClC-2, corresponding to 347 residues (552–898), with forward and reverse primers containing *Bam*HI and *Asc*I restriction sites, respectively. The purified and digested ClC-2ct fragment was cloned into pCMV-75, designed to contain the complete extracellular and transmembrane domains and an eight-residue fragment of the cytoplasmic domain of p75 (Castorino *et al.*, 2011). Single- or double-alanine substitution for leucines, as well as for other residues within ClC-2, ESMI^{623}LL, QVVA^{635}LL, and TIFS^{812}LL motifs, was performed using a QuikChange II site-directed mutagenesis kit (Agilent Technologies, Danbury, CT). Custom-synthesized oligonucleotides were obtained from Thermo Fisher Scientific (Waltham, MA). All constructs were verified by sequencing.

RNA interference

Silencing of μ1A and μ1B in MDCK cells was carried out by electroporation of the following siRNAs: μ1B (AACAAGCTGGTGACTGGCAAA; Gravotta *et al.*, 2007), μ1A (GTGCTCATCTGCCGGAATTTT; Gravotta *et al.*, 2012), or luciferase (GL2; control), all synthesized by Dharmacon (GE Healthcare-Dharmacon, Lafayette, CO). Briefly, a suspension of 4×10^6 of freshly trypsinized MDCK cells in 100 μl of Nucleofector solution V (Lonza, Allendale, NJ), supplemented with 16 pmol of siRNA, was electroporated with the Nucleofector T-23 program (Lonza). This step was then repeated twice at 3-d intervals (Gravotta *et al.*, 2007, 2012). Coupled reverse transcription and PCR (RT-PCR) and Western blot were used to confirm depletion of the targeted molecule.

Cell culture, transient expression, and generation of permanent cell lines

MDCK cells were maintained in growth medium, DMEM (Cellgro) containing 5% fetal bovine serum, at 37°C under 5% CO_2. Transient expression of HA-ClC-2 or p75-ClC-2ct chimeras in MDCK cells was carried out by electroporation-mediated transfection. Briefly, 2×10^6 MDCK cells collected after trypsinization were suspended in 100 μl of Nucleofector solution V containing 5 μg of either pCR3.1(HA-ClC-2) or pCMV(75-ClC-2ct) and electroporated with the Nucleofector T-23 program. Permanent MDCK cell lines expressing either HA-ClC-2 or p75-ClC-2ct were generated by transfecting MDCK cells with Lipofectamine 2000, following manufacturer's recommendations (Life Technologies, Grand Island, NY). Cells expressing the desired proteins were selected in growth medium supplemented with 0.8 mg/ml G418 and isolated with cloning rings.

Immunolabeling and quantification

Immunolabeling of transiently transfected MDCK cells or permanent MDCK cell lines obtained as described was carried out on 12-mm Transwell chambers with 0.4-μm polycarbonate membranes (Costar; Corning, Tewksbury, MA) seeded with 300,000 cells/cm^2 and processed 3.5–4 d after full polarization. Cell surface expression of HA-ClC-2 or chimeras of p75-ClC-2ct was determined by sequential immunolabeling using two different species of antibodies. Cells were rinsed twice at 37°C and once at 4°C with Hank's balanced salt solution (HBSS) containing Ca^{2+} and Mg^{2+} (HBSS-CaMg) and then incubated at 4°C for 30 min with HBSS-CaMg containing 1.5% bovine serum albumin (BSA), followed by the addition of either rat monoclonal antibody against HA or mouse monoclonal antibody against p75 (1/100) and further incubated at 4°C for 4 h to label surface exposed luminal HA epitope in cells expressing HA-ClC-2 or luminal p75 epitopes in cells expressing p75-ClC-2ct chimera (channel 1, intact cells). Cells were rinsed four times with HBSS-CaMg-1.5% BSA and fixed with 3.7% paraformaldehyde for 20 min at 4°C and rinsed, and the aldehyde excess was quenched with 50 mM NH_4Cl in phosphate-buffered saline (PBS) for 20 min at room temperature. Total, intracellular, and surface expression was detected after cell permeabilization with 0.075% saponin in PBS at room temperature for 10 min, followed by a 30-min wash at room temperature with HBSS-CaMg-1.5% BSA and overnight incubation at 4°C with mouse monoclonal antibody against HA or rabbit polyclonal antibody

against p75, respectively (channel 2, permeabilized cells). Excess antibody was eliminated by four rinses with HBSS-CaMg-1.5% BSA. Primary antibodies bound during these sequential incubations were visualized with secondary goat antibodies labeled with Alexa Fluor 488, 568, or 647 (Life Technologies, Carlsbad, CA), as indicated. Cells were then rinsed four times with HBSS-CaMg-1.5% BSA and mounted in Vectashield. Samples were examined with a Zeiss spinning disk confocal microscope equipped with a Yokogawa scanner unit and Zeiss Plan Apochromat 63×/1.46–0.60 oil immersion objective. Confocal image stacks were acquired at 512 × 512 with high-sensitivity Hamamatsu Evolve electron-multiplying charge-coupled device cameras (Photometrics, Tucson, AZ). The acquired image stacks of 90–120 slices ($z = 1$ to $n = 90–120$) were processed to generate regions of interest (ROIs) containing an average of two cells/ROI. The fluorescence images associated with ch2 (labeling all cargoes in permeabilized cells) and ch1 (labeling surface cargoes on intact cells at 4°C) within these ROIs were analyzed with Zen imaging software (Zeiss, Oberkochen, Germany) to generate the following data files:

^{col}Px (surface): pixels within ch2 (permeabilized cells) that *colocalize* with ch1 (intact cells).

$^{col}_{ch2}Mi$: mean intensity of the colocalizing pixels in ch2.

$_{ch2}Px$ (intracellular): pixels within ch2 (permeabilized cells) that *do not colocalize* with ch1 (intact cells).

$_{ch2}Mi$: mean intensity of the noncolocalizing pixels in ch2.

The following equations are operators that sum the product of pixel number (*Px*) and the mean intensity (*Mi*) within an ROI for all $z = 1 – n$ slices of each image stack:

For surface total (S_t; colocalized),

$$S_t = \sum_{z=1}^{n} \left[{}^{col}Px \times {}^{col}_{ch2}Mi \right]$$

For intracellular total (IC_t; not-colocalized),

$$IC_t = \sum_{z=1}^{n} \left[{}_{ch2}Px \times {}_{ch2}Mi \right]$$

The values obtained represent total surface (S_t) and total intracellular (IC_t) cargoes. The fraction of total cargo on the surface versus intracellular pools, represented in the bar graphs of Figures 3–5 and Supplemental Figure S2, is calculated as follows:

Surface (fraction of total) = $S_t/S_t + IC_t$

Intracellular (fraction of total) = $IC_t/S_t + IC_t$

Statistical analyses

Data derived from images collected and processed as described were analyzed by one-way ANOVA to obtained mean, SD, and probability (*p*) values. The *p* values obtained were subjected to multiple hypothesis testing using Bonferroni's corrections. All analyses were performed with statistical software Origin9.1 (OriginLab, Northampton, MA).

Molecular modeling of ClC-2 and the interactions of its ESMI^{623}LL motif with AP-1

The comparative modeling of human ClC-2 was performed using the MODELLER program (Webb and Sali, 2014) as implemented in the Build Homology Model module of Discovery Studio, version 2.1 software (Accelrys, San Diego, CA). We used a suitable template for modeling ClC-2 (Uniprot, P51788) the crystal structure of *Cyanidioschyzon merolae* eukaryotic ClC transporter (CmClC; Protein Data Bank [PDB] 3ORG, at 3.5-Å resolution; Feng *et al*., 2010). The missing extracellular loop residues were constructed using bacterial ClCs (PDB IDs 1OTS, 1KPL; Dutzler *et al*., 2002, 2003). The CBS domains of ClC-2 were modeled using the reported structures of cytoplasmic domains of ClC-Ka (PDB 2PFI; Markovic and Dutzler, 2007) and ClC-0 (PDB 2D4Z). Using the previously completed CmClC structure, the sequence alignment considered secondary structure predictions and PFAM sequence conservation for domains CLC (PF00654) and CBS (PF00571). For modeling purposes, the first 83 residues and those corresponding to segments 663–694 and 725–771 were not included due to lack of an appropriate template. The protein was modeled as a dimer, and 100 models were generated; the best model ranked by MODELLER (internal PDF score) was energy minimized using the conjugate gradient algorithm until a root mean square (RMS) gradient of 0001 kcal/mol Å was reached. The CHARMM22 force field with a dielectric constant of 4 and a distance-dependent dielectric implicit solvent model to mimic the membrane environment was used (Brooks *et al*., 2009). Model quality assessment was performed using the SAVES server (http://nihserver.mbi.ucla.edu/SAVES/), which indicates that the obtained model has >95% of residues in the allowed regions according to Ramachandran plot analysis.

We modeled the active AP-1A complex interacting with the canonical dileucine motif present in CD4 cocrystallized with AP2 (PDB ID 2JKR; Kelly *et al*., 2008; Jackson *et al*., 2010). Accordingly, we proposed that AP-1A might interact with the dileucine motif ESMI^{623}LL of CBS1. Thus we modeled the interaction between the dileucine-binding pocket in the γ1–σ1A heterocomplex of AP-1 and a ClC-2 617–621 peptide containing the ESMI^{623}LL dileucine motif (SPESMI^{623}LLG). The obtained complex was relaxed using molecular mechanics minimization using the CHARMM22 force field in Discovery Studio, version 2.1, using the conjugate gradient algorithm with a distance-dependent dielectric implicit solvent model with a dielectric constant of 80 until a RMS gradient of 0.0001 kcal/mol Å was reached.

Yeast three-hybrid assays

The C-cytoplasmic domain of ClC-2 was amplified and cloned into the multiple cloning site 1 (MCS-1) of pBridge vector (Clontech, Mountain View, CA) using *Eco*RI and *Sal*I restriction sites. A cDNA encoding σ1A subunit was cloned into the MCS-2 (GAL4-BD) of pBridge using the *Not*I and *Bgl*II restriction sites. The constructs containing β1 subunit (GAL4-AD-β) or γ1 subunit (GAL4-AD-γ) were gifts from J. S. Bonifacino (National Institute of Child Health and Human Development, Bethesda, MD; Janvier *et al*., 2003). Alanine substitution of selected residues within σ1A, ^{65}L/S, ^{88}V/D, and ^{98}V/S was performed using a QuikChange II site-directed mutagenesis kit with custom-synthesized oligonucleotides from Fisher-Scientific. Yeast three-hybrid assays were carried out with strain HF7c (Clontech) as reported previously (Janvier *et al*., 2003) using a lithium acetate transformation protocol (Clontech). Transformed HF7c cells were selected in medium lacking leucine, tryptophan, and methionine (DOB-3). Bait–prey interaction was determined by spotting transformed cells from diluted samples (0.05 OD_{600}) on plates lacking tryptophan, leucine, methionine, and histidine (DOB-4) after 4–6 d of incubation at 30°C. Plates were recorded with a scanner (model 3200; Epson). Quantitative assays were carried out by growing transformed cells in liquid medium (DOB-4) by duplicate for 5–6 d monitoring OD_{600} at indicated intervals.

Lentivirus generation and cell transduction

Wild-type and mutant forms of CLC2-HA were subcloned in the pCCL-PGK lentiviral vector (kindly provided by Shahin Rafii, Weill Cornell Medical College [WCMC], New York, NY), and lentiviruses were generated as previously described (Seandel *et al*., 2008).

Viral supernatants were concentrated 100-fold with the Lenti-X Concentrator (Clontech) following the manufacturer's instructions. For viral titration, total RNA was isolated from the concentrated viral preparations with the RNeasy Mini Kit (Quiagen, Valencia, CA), including an in-column DNase digestion step. Viral RNA was converted to cDNA with the High Capacity cDNA Reverse Transcription Kit (Life Technologies) and quantified in a StepOnePlus Real-Time PCR System (Life Technologies) using SYBR Select Master Mix (Life Technologies) and HIV RRE-specific primers (5′-GTATAGTGCAGCAGCAGAAC-3′ and 5′-ACAGCAGTGGTGCAAATGAG-3′). Quantification was performed by interpolation into a standard curve.

For cell transduction, 1.5×10^5 MDCK cells were seeded on 12-mm Transwell chambers with 0.4-μm-pore polycarbonate membranes (Costar). After 24 h, 50 viral genome equivalents/cell were added to the top chamber in the presence of 6 μg/ml Polybrene (Sigma-Aldrich, St. Louis, MO), and the inoculum was replaced by fresh medium 24 h later. Three days later, fully polarized cells were processed for further analysis.

Domain-selective biotinylation and SBAS

Cell surface biotinylation and SBAS assays were carried out as previously described (Gravotta *et al.*, 2012). This assay, in contrast to the conventional surface domain biotinylation-streptavidin retrieval assay (Sargiacomo *et al.*, 1989), quantifies the steady-state apical/basolateral surface distribution of a given protein as a fraction of the total protein pool. Briefly, fully polarized MDCK monolayers seeded at 300,000 cells/cm^2 on 0.4-μm polycarbonate membranes in 12-mm Transwell chambers were subjected to domain-selective biotinylation using sulfo-NHS-LC-biotin twice for 20 min at 4°C, either apically or basolaterally. Identical (60 μl) aliquots of a lysate made in 40 mM Tris-HCl, pH 7.8, 5 mM EDTA, and 1% SDS containing a protease inhibitor cocktail were supplemented with 25 mM dithiothreitol and heated at 65°C for 10 min, mixed with 55 μl of a buffer containing 500 μg/ml avidin, 35% glycerol, and 15 μg/ml bromophenol blue, supplemented with 1.2 mM biotin (biotin+) or not (biotin–), and heated at 65°C for 10 min (Gravotta *et al.*, 2012). Samples were resolved side by side by SDS–PAGE, processed for Western blot with antibodies against cargo proteins, and quantified using ECL (GE Healthcare-Dharmacon) or Odyssey (LI-COR Bioscience, Lincoln, NE).

Under the conditions of this assay, the intensity differences between the electrophoretic gel bands in biotin+ and biotin– samples represent the pool of biotinylated cargo molecules localized at apical (AP) and basolateral (BL) domains as a fraction of the total cargo pool (Gravotta *et al.*, 2012):

For apically biotinylated cells,

$$\text{AP-cargo} = [(\text{biotin+}) - (\text{biotin–})]/(\text{biotin+})$$

For basolaterally biotinylated cells,

$$\text{BL-cargo} = [(\text{biotin+}) - (\text{biotin–})]/(\text{biotin+})$$

Intracellular cargo is calculated as

$$\text{IC-cargo} = 1 - (\text{AP-cargo} - \text{BL-cargo})$$

Immunoprecipitation

MDCK cells expressing GFP-ClC-2 were lysed at 4°C with lysis buffer (1% Triton X-100, 25 mM Tris-Cl, pH 7.5, 150 mM NaCl, 0.5 mM EDTA, 10% glycerol) and a cocktail of protease inhibitors. The lysate was precleared by centrifugation at 10,000 rpm for 15 min and the supernatant incubated with 1.5 μg of mouse anti–γ-adaptin antibody absorbed to 50 μl of Dynabeads (Life Technologies, Carlsbad, CA) for 3 h at 4°C. The immunocomplexes were washed five times with lysis buffer and once with wash buffer in Dynabead kit and eluted with 3.6× Laemmli sample buffer. The samples were heated at 70°C for 10 min, resolved by 4-12% SDS–PAGE, and processed for Western blot with either primary mouse anti–γ-adaptin or chicken anti-GFP antibodies, followed by secondary antibodies labeled with red IRDye^{680} (anti-mouse) and green IRDye^{800} (anti-chicken) and imaged using Odyssey.

ACKNOWLEDGMENTS

We thank Alessio Accardi, Department of Physiology and Biophysics, WCMC, and David Eliezer, Department of Biochemistry, WCMC, for critical reading of the manuscript and Alan Weinstein, Department of Physiology and Biophysics. WCMC, for advice with mathematical formulas. This work was supported by National Institutes of Health Grants GM34107 and EY08531 to E.R.B., a Beca-Chile fellowship to E.F.-O., a Pew Latin American Fellowship to G.L., and the Dyson Foundation and the Research to Prevent Blindness Foundation.

REFERENCES

Bello V, Goding JW, Greengrass V, Sali A, Dubljevic V, Lenoir C, Trugnan G, Maurice M (2001). Characterization of a di-leucine-based signal in the cytoplasmic tail of the nucleotide-pyrophosphatase NPP1 that mediates basolateral targeting but not endocytosis. Mol Biol Cell 12, 3004–3015.

Blaisdell CJ, Edmonds RD, Wang XT, Guggino S, Zeitlin PL (2000). pH-regulated chloride secretion in fetal lung epithelia. Am J Physiol Lung Cell Mol Physiol 278, L1248–L1255.

Bonifacino JS (2014). Adaptor proteins involved in polarized sorting. J Cell Biol 204, 7–17.

Bonifacino JS, Traub LM (2003). Signals for sorting of transmembrane proteins to endosomes and lysosomes. Annu Rev Biochem 72, 395–447.

Bosl MR, Stein V, Hubner C, Zdebik AA, Jordt SE, Mukhopadhyay AK, Davidoff MS, Holstein AF, Jentsch TJ (2001). Male germ cells and photoreceptors, both dependent on close cell-cell interactions, degenerate upon ClC-2 Cl(-) channel disruption. EMBO J 20, 1289–1299.

Brooks BR, Brooks CL 3rd, Mackerell AD Jr, Nilsson L, Petrella RJ, Roux B, Won Y, Archontis G, Bartels C, Boresch S, *et al.* (2009). CHARMM: the biomolecular simulation program. J Comput Chem 30, 1545–1614.

Carvajal-Gonzalez JM, Gravotta D, Mattera R, Diaz F, Perez Bay A, Roman AC, Schreiner RP, Thuenauer R, Bonifacino JS, Rodriguez-Boulan E (2012). Basolateral sorting of the coxsackie and adenovirus receptor through interaction of a canonical YXXPhi motif with the clathrin adaptors AP-1A and AP-1B. Proc Natl Acad Sci USA 109, 3820–3825.

Castorino JJ, Deborde S, Deora A, Schreiner R, Gallagher-Colombo SM, Rodriguez-Boulan E, Philp NJ (2011). Basolateral sorting signals regulating tissue-specific polarity of heteromeric monocarboxylate transporters in epithelia. Traffic 12, 483–498.

Catalán M, Cornejo I, Figueroa CD, Niemeyer MI, Sepúlveda FV, Cid LP (2002). ClC-2 in guinea pig colon: mRNA, immunolabeling, and functional evidence for surface epithelium localization. Am J Physiol Gastrointest Liver Physiol 283, G1004–G1013.

Catalán M, Niemeyer MI, Cid LP, Sepúlveda FV (2004). Basolateral ClC-2 chloride channels in surface colon epithelium: regulation by a direct effect of intracellular chloride. Gastroenterology 126, 1104–1114.

Cornejo I, Niemeyer MI, Zuniga L, Yusef YR, Sepulveda F V, Cid LP (2009). Rapid recycling of ClC-2 chloride channels between plasma membrane and endosomes: role of a tyrosine endocytosis motif in surface retrieval. J Cell Physiol 221, 650–657.

Deborde S, Perret E, Gravotta D, Deora A, Salvarezza S, Schreiner R, Rodriguez-Boulan E (2008). Clathrin is a key regulator of basolateral polarity. Nature 452, 719–723.

Diaz F, Gravotta D, Deora A, Schreiner R, Schoggins J, Falck-Pedersen E, Rodriguez-Boulan E (2009). Clathrin adaptor AP1B controls adenovirus infectivity of epithelial cells. Proc Natl Acad Sci USA 106, 11143–11148.

Doray B, Lee I, Knisely J, Bu G, Kornfeld S (2007). The gamma/sigma1 and alpha/sigma2 hemicomplexes of clathrin adaptors AP-1 and AP-2 harbor the dileucine recognition site. Mol Biol Cell 18, 1887–1896.

Doumanov JA, Daubrawa M, Unden H, Graeve L (2006). Identification of a basolateral sorting signal within the cytoplasmic domain of the interleukin-6 signal transducer gp130. Cell Signal 18, 1140–1146.

Dutzler R, Campbell EB, Cadene M, Chait BT, MacKinnon R (2002). X-ray structure of a ClC chloride channel at 3.0 A reveals the molecular basis of anion selectivity. Nature 415, 287–294.
Dutzler R, Campbell EB, MacKinnon R (2003). Gating the selectivity filter in ClC chloride channels. Science 300, 108–112.
Edwards MM, Marín de Evsikova C, Collin GB, Gifford E, Wu J, Hicks WL, Whiting C, Varvel NH, Maphis N, Lamb BT, *et al.* (2010). Photoreceptor degeneration, azoospermia, leukoencephalopathy, and abnormal RPE cell function in mice expressing an early stop mutation in CLCN2. Invest Ophthalmol Vis Sci 51, 3264–3272.
Feng L, Campbell EB, Hsiung Y, MacKinnon R (2010). Structure of a eukaryotic CLC transporter defines an intermediate state in the transport cycle. Science 330, 635–641.
Fölsch H, Ohno H, Bonifacino JS, Mellman I (1999). A novel clathrin adaptor complex mediates basolateral targeting in polarized epithelial cells. Cell 99, 189–198.
Gan Y, McGraw TE, Rodriguez-Boulan E (2002). The epithelial-specific adaptor AP1B mediates post-endocytic recycling to the basolateral membrane. Nat Cell Biol 4, 605–609.
Garcia-Olivares J, Alekov A, Boroumand MR, Begemann B, Hidalgo P, Fahlke C (2008). Gating of human ClC-2 chloride channels and regulation by carboxy-terminal domains. J Physiol 586, 5325–5336.
Gonzalez A, Rodriguez-Boulan E (2009). Clathrin and AP1B: key roles in basolateral trafficking through trans-endosomal routes. FEBS Lett 583, 3784–3795.
Gravotta D, Carvajal-Gonzalez JM, Mattera R, Deborde S, Banfelder JR, Bonifacino JS, Rodriguez-Boulan E (2012). The clathrin adaptor AP-1A mediates basolateral polarity. Dev Cell 22, 811–823.
Gravotta D, Deora A, Perret E, Oyanadel C, Soza A, Schreiner R, Gonzalez A, Rodriguez-Boulan E (2007). AP1B sorts basolateral proteins in recycling and biosynthetic routes of MDCK cells. Proc Natl Acad Sci USA 104, 1564–1569.
Greenough M, Pase L, Voskoboinik I, Petris MJ, O'Brien AW, Camakaris J (2004). Signals regulating trafficking of Menkes (MNK; ATP7A) copper-translocating P-type ATPase in polarized MDCK cells. Am J Physiol Cell Physiol 287, C1463–C1471.
Gründer S, Thiemann A, Pusch M, Jentsch TJ (1992). Regions involved in the opening of CIC-2 chloride channel by voltage and cell volume. Nature 360, 759–762.
Guezguez B, Vigneron P, Alais S, Jaffredo T, Gavard J, Mege RM, Dunon D (2006). A dileucine motif targets MCAM-l cell adhesion molecule to the basolateral membrane in MDCK cells. FEBS Lett 580, 3649–3656.
Gyömörey K, Yeger H, Ackerley C, Garami E, Bear CE (2000). Expression of the chloride channel ClC-2 in the murine small intestine epithelium. Am J Physiol Cell Physiol 279, C1787–C1794.
Hohberger B, Enz R (2009). Cereblon is expressed in the retina and binds to voltage-gated chloride channels. FEBS Lett 583, 633–637.
Hunziker W, Fumey C (1994). A di-leucine motif mediates endocytosis and basolateral sorting of macrophage IgG Fc receptors in MDCK cells. EMBO J 13, 2963–2969.
Jackson LP, Kelly BT, McCoy AJ, Gaffry T, James LC, Collins BM, Höning S, Evans PR, Owen DJ (2010). A large-scale conformational change couples membrane recruitment to cargo binding in the AP2 clathrin adaptor complex. Cell 141, 1220–1229.
Janvier K, Kato Y, Boehm M, Rose JR, Martina JA, Kim BY, Venkatesan S, Bonifacino JS (2003). Recognition of dileucine-based sorting signals from HIV-1 Nef and LIMP-II by the AP-1 gamma-sigma1 and AP-3 delta-sigma3 hemicomplexes. J Cell Biol 163, 1281–1290.
Jentsch TJ (2002). Chloride channels are different. Nature 415, 276–277.
Jentsch TJ (2005). Chloride transport in the kidney: lessons from human disease and knockout mice. J Am Soc Nephrol 16, 1549–1561.
Jentsch TJ (2008). CLC chloride channels and transporters: from genes to protein structure, pathology and physiology. Crit Rev Biochem Mol Biol 43, 3–36.
Jentsch TJ, Maritzen T, Zdebik AA (2005). Chloride channel diseases resulting from impaired transepithelial transport or vesicular function. J Clin Invest 115, 2039–2046.
Jeworutzki E, López-Hernández T, Capdevila-Nortes X, Sirisi S, Bengtsson L, Montolio M, Zifarelli G, Arnedo T, Müller CS, Schulte U, *et al.* (2012). GlialCAM, a protein defective in a leukodystrophy, serves as a ClC-2 Cl(-) channel auxiliary subunit. Neuron 73, 951–961.
Johnson KF, Kornfeld S (1992). The cytoplasmic tail of the mannose 6-phosphate/insulin-like growth factor-II receptor has two signals for lysosomal enzyme sorting in the Golgi. J Cell Biol 119, 249–257.
Kelly BT, McCoy AJ, Spate K, Miller SE, Evans PR, Honing S, Owen DJ (2008). A structural explanation for the binding of endocytic dileucine motifs by the AP2 complex. Nature 456, 976–979.
Le Gall AH, Powell SK, Yeaman CA, Rodriguez-Boulan E (1997). The neural cell adhesion molecule expresses a tyrosine-independent basolateral sorting signal. J Biol Chem 272, 4559–4567.
Letourneur F, Klausner RD (1992). A novel di-leucine motif and a tyrosine-based motif independently mediate lysosomal targeting and endocytosis of CD3 chains. Cell 69, 1143–1157.
Ling K, Bairstow SF, Carbonara C, Turbin DA, Huntsman DG, Anderson RA (2007). Type I gamma phosphatidylinositol phosphate kinase modulates adherens junction and E-cadherin trafficking via a direct interaction with mu 1B adaptin. J Cell Biol 176, 343–353.
Lipecka J, Bali Z, Thomas A, Fanen P, Edelman A, Fritsch J, Distri- JF (2002). Distribution of ClC-2 chloride channel in rat and human epithelial tissues. Am J Physiol Cell Physiol 282, C805–C816.
Ma D, Taneja TK, Hagen BM, Kim BY, Ortega B, Lederer WJ, Welling PA (2011). Golgi export of the Kir2.1 channel is driven by a trafficking signal located within its tertiary structure. Cell 145, 1102–1115.
Markovic S, Dutzler R (2007). The structure of the cytoplasmic domain of the chloride channel ClC-Ka reveals a conserved interaction interface. Structure 15, 715–725.
Mattera R, Boehm M, Chaudhuri R, Prabhu Y, Bonifacino JS (2011). Conservation and diversification of dileucine signal recognition by adaptor protein (AP) complex variants. J Biol Chem 286, 2022–2030.
Miranda KC, Khromykh T, Christy P, Le TL, Gottardi CJ, Yap AS, Stow JL, Teasdale RD (2001). A dileucine motif targets E-cadherin to the basolateral cell surface in Madin-Darby canine kidney and LLC-PK1 epithelial cells. J Biol Chem 276, 22565–22572.
Murray CB, Morales MM, Flotte TR, McGrath-Morrow SA, Guggino WB, Zeitlin PL (1995). ClC-2: a developmentally dependent chloride channel expressed in the fetal lung and downregulated after birth. Am J Respir Cell Mol Biol 12, 597–604.
Nakatsu F, Hase K, Ohno H (2014). The role of the clathrin adaptor AP-1: polarized sorting and beyond. Membranes (Basel) 4, 747–763.
Nehrke K, Arreola J, Nguyen H-V, Pilato J, Richardson L, Okunade G, Baggs R, Shull GE, Melvin JE (2002). Loss of hyperpolarization-activated Cl(-) current in salivary acinar cells from Clcn2 knockout mice. J Biol Chem 277, 23604–23611.
Nemer W El, Colin Y, Bauvy C, Codogno P, Fraser RH, Cartron JP, Le C, Kim V (1999). Isoforms of the Lutheran/basal cell adhesion molecule glycoprotein are differentially delivered in polarized epithelial cells. J Biol Chem 274, 31903–31908.
Newton EE, Wu Z, Simister NE (2005). Characterization of basolateral-targeting signals in the neonatal Fc receptor. J Cell Sci 118, 2461–2469.
Ohno H, Tomemori T, Nakatsu F, Okazaki Y, Aguilar RC, Foelsch H, Mellman I, Saito T, Shirasawa T, Bonifacino JS (1999). Mu1B, a novel adaptor medium chain expressed in polarized epithelial cells. FEBS Lett 449, 215–220.
Peña-Münzenmayer G, Catalán M, Cornejo I, Figueroa CD, Melvin JE, Niemeyer MI, Cid LP, Sepúlveda F V (2005). Basolateral localization of native ClC-2 chloride channels in absorptive intestinal epithelial cells and basolateral sorting encoded by a CBS-2 domain di-leucine motif. J Cell Sci 118, 4243–4252.
Poyatos I, Ruberti F, Martínez-Maza R, Giménez C, Dotti CG, Zafra F (2000). Polarized distribution of glycine transporter isoforms in epithelial and neuronal cells. Mol Cell Neurosci 15, 99–111.
Puertollano R, Aguilar RC, Gorshkova I, Crouch RJ, Bonifacino JS (2001). Sorting of mannose 6-phosphate receptors mediated by the GGAs. Science 292, 1712–1716.
Regeer RR, Markovich D (2004). A dileucine motif targets the sulfate anion transporter sat-1 to the basolateral membrane in renal cell lines. Am J Physiol Cell Physiol 287, C365–C372.
Sargiacomo M, Lisanti M, Graeve L, Le Bivic A, Rodriguez-Boulan E (1989). Integral and peripheral protein compositions of the apical and basolateral membrane domains in MDCK cells. J Membr Biol 107, 277–286.
Schreiner R, Frindt G, Diaz F, Carvajal-Gonzalez JM, Perez Bay AE, Palmer LG, Marshansky V, Brown D, Philp NJ, Rodriguez-Boulan E (2010). The absence of a clathrin adapter confers unique polarity essential to proximal tubule function. Kidney Int 78, 382–388.
Seandel M, Butler JM, Kobayashi H, Hooper AT, White IA, Zhang F, Vertes EL, Kobayashi M, Zhang Y, Shmelkov SV, *et al.* (2008). Generation of a

functional and durable vascular niche by the adenoviral E4ORF1 gene. Proc Natl Acad Sci USA 105, 19288–19293.
Simonsen A, Stang E, Bremnes B, Røe M, Prydz K, Bakke O (1997). Sorting of MHC class II molecules and the associated invariant chain (Ii) in polarized MDCK cells. J Cell Sci 110 (Pt 5), 597–609.
Stauber T, Jentsch TJ (2010). Sorting motifs of the endosomal/lysosomal CLC chloride transporters. J Biol Chem 285, 34537–34548.
Strange K (2011). Putting the pieces together: a crystal clear window into CLC anion channel regulation. Channels 5, 101–105.
Strauss O (2005). The retinal pigment epithelium in visual function. Physiol Rev 85, 845–881.
Stölting G, Fischer M, Fahlke C (2014). CLC channel function and dysfunction in health and disease. Front Physiol 5, 378.
Thiemann A, Gründer S, Pusch M, Jentsch TJ (1992). A chloride channel widely expressed in epithelial and non-epithelial cells. Nature 356, 57–60.
Traub LM (2009). Tickets to ride: selecting cargo for clathrin-regulated internalization. Nat Rev Mol Cell Biol 10, 583–596.
Webb B, Sali A (2014). Comparative protein structure modeling using MODELLER. Curr Protoc Bioinformatics 47, 5.6.1–5.6.32.
Yeaman C, Le Gall AH, Baldwin AN, Monlauzeur L, Le Bivic A, Rodriguez-Boulan E (1997). The O-glycosylated stalk domain is required for apical sorting of neurotrophin receptors in polarized MDCK cells. J Cell Biol 139, 929–940.
Zhu Y, Doray B, Poussu A, Lehto VP, Kornfeld S (2001). Binding of GGA2 to the lysosomal enzyme sorting motif of the mannose 6- phosphate receptor. Science 292, 1716–1718.